POLITECNICO DI TORINO

Master's Degree in Aerospace Engineering

Master's Degree Thesis

Multiple Near-Earth Asteroids rendezvous trajectories optimization using Electric Propulsion

Supervisor

Lorenzo CASALINO

Candidate

Cosimo Luigi MAI

April 2022

Abstract

Space missions require fuel to be expended, and every kilogram of fuel on-board is a kilogram of scientific equipment sacrificed to preserve the mission feasibility. The ability to optimize the spacecraft trajectory by minimizing fuel is key to greater scientific return. In some cases, this becomes the only way for the desired mission to succeed.

This thesis investigates the problem of trajectory optimization for the case of multiple Near-Earth Asteroids (NEAs) rendezvous missions using Electric Propulsion (EP). NEAs are of fundamental interest for the understanding of our solar system as well as for planetary defence and are stepping stones for interplanetary human flight. Close-up observations of these objects will drastically increase our knowledge about the overall NEA population. Furthermore, low-thrust EP represents a viable option for these missions, offering a higher efficiency compared to chemical propulsion.

To solve the optimization problem an indirect approach is adopted. This allows for an exact, even though numerical, optimization and presents a lower computational cost compared to direct methods. However, the capability of achieving an accurate result is highly dependent on the tentative solution.

In this study suitable procedures to overcome convergence difficulties and to find low-cost optimized solutions are described. Examples show that by applying these procedures, the derivation of tentative solutions sufficiently close to the optimal ones is straightforward, resulting in a faster convergence to the optimum.

I

Acknowledgements

In primo luogo un ringraziamento sincero al professor Lorenzo Casalino: le sue indicazioni e il suo supporto sono stati di fondamentale importanza per la riuscita di questo lavoro di tesi. Il suo atteggiamento di assoluta disponibilità e apertura sono stati per me innanzitutto un forte insegnamento umano, per cui gli sono molto grato.

Vorrei inoltre ringraziare tutta la mia famiglia, per il suo sostegno dolce e incondizionato. Un pensiero particolare per mia madre, mio punto di riferimento fermo e costante; insegnante di lettere e storia per professione ma ormai espertissima ingegnere aerospaziale, tante sono state le volte che ha ascoltato i miei dubbi nel corso degli anni universitari. A lei devo moltissimo; rappresenta per me il sostegno che permette di affrontare con serenità e fermezza le cose quotidiane. Il confronto che contraddistingue il nostro rapporto è una fonte inesauribile per la mia continua crescita.

Un grazie enorme anche a mia sorella, che mi sprona e mi dà coraggio in ogni situazione. Rappresenta per me la luce più brillante nei momenti più difficili e la migliore compagna di giochi nei momenti di leggerezza. Dolce, tenace, schietta, onesta, ogni confronto con lei mi permette di allargare i miei orizzonti e di ridimensionare le preoccupazioni del quotidiano.

Grazie a Peppe, per il supporto costante e per il confronto sempre sincero. Grazie per tutti gli insegnamenti e per avermi sempre trasmesso una grandissima curiosità verso tutto ciò di cui facciamo esperienza. Grazie, in particolare, per avermi fatto capire la bellezza e la complessità della natura.

Un grazie sincero a mio padre, il cui insegnamento più grande rimane per me quello di concentrarsi quanto più possibile sulla positività che, in ogni sua forma, ci circonda. La leggerezza, "che non è superficialità, ma planare sulle cose dall'alto, non avere macigni sul cuore" - come scrive Calvino - e la grande felicità ed emozione per le cose più piccole, hanno sempre costituito per me un esempio da seguire.

Vorrei esprimere infine l'immensa gratitudine che provo nei confronti dei miei amici. Grazie per il nostro tempo insieme, nell'affrontare momenti complessi e momenti leggeri, grazie per il nostro confronto, grazie per la vostra vicinanza,

Table of Contents

List of Tables

List of Figures

Chapter 1

Introduction

An outline that categorizes the key elements within the general process of spacecraft trajectory optimization is presented. After that, the problem statement and the thesis objective are provided. Finally, the thesis overview is given.

The following chapter's theoretical principles are primarily based on the research of doctor Shirazi and professors Ceberio and Lozano [1], and professor Conway [2].

1.1 Spacecraft trajectory optimization

The subject of spacecraft trajectory optimization has a long and interesting history. The general theoretical framework for optimal control applied to spacecraft trajectory optimization is completely presented in the pioneering work by Lawden [3].

The problem can be simply stated as the determination of a trajectory for a spacecraft that satisfies specified initial and terminal conditions, that is conducting a required mission, while minimizing some quantity of importance. The most common objective is to minimize the propellant required or equivalently to maximize the fraction of the spacecraft that is not devoted to propellant [2].

The overall strategy for addressing a spacecraft trajectory optimization problem can be split into four steps:

- mathematical modeling of system dynamics;

- defining appropriate objectives;

- developing an approach;

- achieving a solution.

These steps are represented by model, objective, approach and solution respectively. On the other hand, each space mission is characterized by several factors: mission requirements, goals, expected accuracy, desired convergence, mission plan, etc. Each of these aspects affects the steps of the mentioned process differently [1].
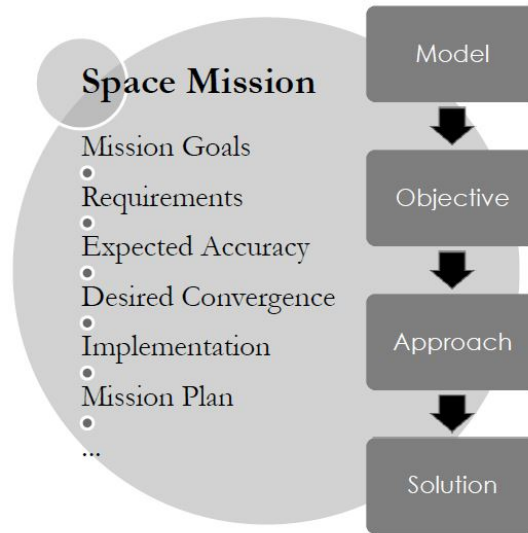
Figure 1.1: General scheme of spacecraft trajectory optimization process [1]

The first step involves not just a spacecraft trajectory optimization problem but any orbital mechanics problem. First and foremost, a solid understanding of the system's dynamics is required. The mathematical model of the problem can then be derived, which involves selecting a set of states to represent the system and deriving motion equations for the spacecraft.

The second step prescribes the definition of a *performance index* or *cost function* that considers a series of mission objectives identified during the mission design process. Typical mission objectives are:

1. minimize transfer time for a given payload or propellant mass;

2. minimize propellant mass for a given mission transfer time and lauch mass;

3. minimize propellant mass for a given mission transfer time and payload mass.

In practice, spacecraft trajectories have to be optimized with respect to several conflicting mission objectives, e.g. minimize transfer time and propellant mass. Such multi-objective optimization problems are usually reformulated as a series of single-objective problems [4].

The third step refers to the type of methods and techniques which are dedicated to solving the trajectory design problem. The approach can be divided into two categories: analytical and numerical.

The fourth step is to solve the problem regarding the developed approach. If the analytical approach is developed in the third step, the solution is likely to be a closed

form analytical solution. However, if the numerical approach is used, the problem usually turns into a black-box optimization problem and needs numerical algorithms to achieve a solution. The majority of spacecraft trajectory optimization problems end up in the latter form. The reason is that a typical spacecraft optimization problem does not have a closed form solution due to its nonlinearity, unless specific conditions and assumptions are considered in the approach. Such assumptions may limit the matching between simulation and reality in spacecraft motion [1].

1.1.1 Model

The mathematical modeling of the spacecraft dynamics is the first step in the trajectory optimization process. A set of ordinary differential equations can be used to describe the spacecraft trajectory, providing the time history of the spacecraft's position and velocity. Mathematically, these equations can be expressed as:

$$\dot{\mathbf{x}} = \mathbf{f}(\mathbf{x}(t), \mathbf{u}(t), t) \tag{1.1}$$

where t represents the time, $\dot{\mathbf{x}}(t)$ is an n-dimensional time history of the state vector and $\mathbf{u}(t)$ is an m-dimensional time history of the control vector. The state vector generally includes the spacecraft's position and velocity vectors, while the control vector represents the system input. The mathematical model can be generally categorized based on a variety of features.
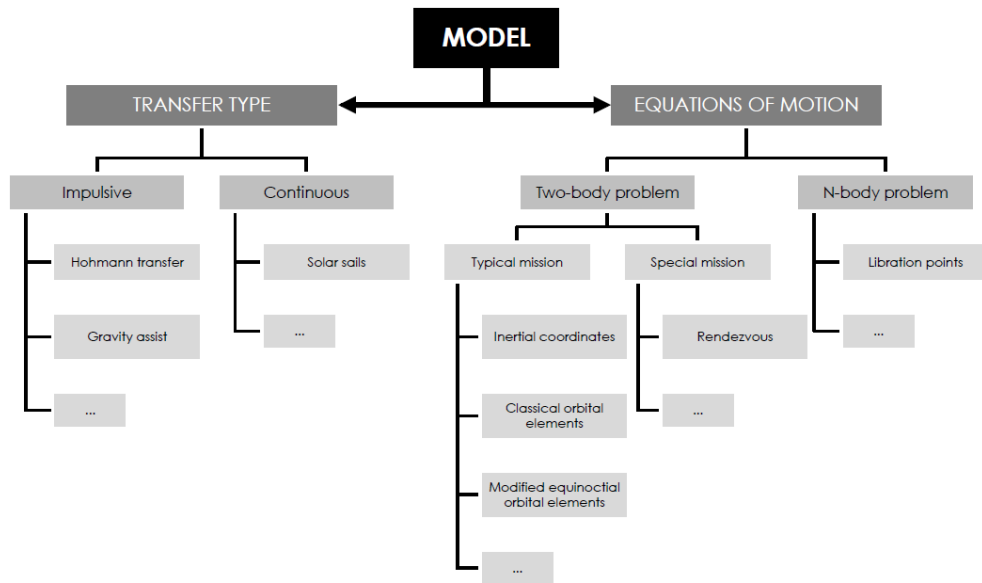
Figure 1.2: Taxonomy of mathematical models in spacecraft trajectory optimization [1]

Figure 1.2 depicts the general classification of mathematical models used in space-craft trajectory optimization. Two categories can be identified:

- *Models based on transfer type*, where the simulation of system inputs is the primary concern. Within this category, the mathematical model can be either *impulsive* or *continuous*, depending on the analysed space mission.

  - *Impulsive model.* The system inputs are assumed to be zero $\mathbf{u}(t) = 0$, and the spacecraft maneuvers are modeled as sudden velocity increments ($\Delta V > 0$), that is, considering zero burn time ($\Delta t = 0$). This model is typically helpful when engines with relatively low specific impulse (I_{sp}) and high thrust levels are used, i.e. when high-thrust chemical propulsion is employed.

  - *Continuous model.* The spacecraft trajectory is modeled considering non-zero inputs ($\mathbf{u}(t) \neq 0$). Thus, this model results more complicated but also more precise with respect to the impulsive one. This mathematical representation is frequently used in the analysis of low-thrust space missions.

- *Models based on equations of motion*, where the formulation of the differential equations set ($\mathbf{f}(\mathbf{x}(t), \mathbf{u}(t), t)$) is the matter of interest. The representation of the dynamics of spacecraft motion can be divided into two major categories, depending on the analysed space missions: *two-body problems* and *N-body problems*.

  - *Two-body problems.* These kinds of models consider two point masses and define their mutual gravitational attraction, assuming the spacecraft's mass is significantly smaller than the mass of the body it is orbiting. This allows the mass of the spacecraft and its gravitational effects on the larger body to be ignored.

  - *N-body problems.* The gravitational influence of more than one celestial body is considered on the spacecraft within these models. For instance, simulations of transfers to the *Lagrange's points* exploit the Circular Restricted Three-Body Problem, which is the simplest model to investigate the three-body problem.

Clearly, these categories are not mutually exclusive; for example, one can simulate two-body or N-body problems using either impulsive or continuous models.

1.1.2 Objective

The second critical step in the spacecraft trajectory optimization process is to define an objective function, based on space mission requirements. The general

form of the objective function, also known as Bolza cost function, can be expressed as:

$$J(\mathbf{x}, \mathbf{u}, t) = \varphi(\mathbf{x}(t_f), t_f) + \int_{t_0}^{t_f} \Phi(\mathbf{x}(t), \mathbf{u}(t), t)\mathrm{d}t \qquad (1.2)$$

where t_0 and t_f represent the initial and the final time, respectively. The function φ is the *Mayer* term and indicates the cost related to the final states, while Φ is the *Lagrange* term which depends on the state's and the controls' time history. Depending on what is being optimized, the objective function can contain both the Lagrange and the Mayer terms, or just one of them. Figure 1.3 shows a typical classification of objective functions, which considers *type* and *quantity*:
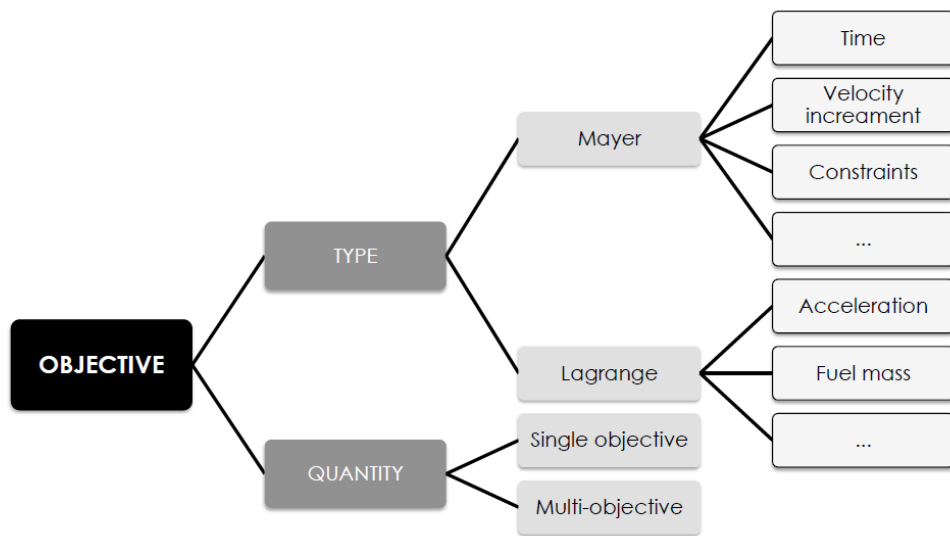
Figure 1.3: Taxonomy of objectives in spacecraft trajectory optimization [1]

As mentioned, Mayer or Lagrange term can be chosen to express the objective function. Moreover, cost functions can be categorized according to the number of objective they include; in particular, a distinction can be made between single objective and multi-objective ones. Single objective cost functions consider a single criterion, while multi-objective cost functions involves several distinct criteria. In these cases, the most straightforward approach to the spacecraft optimization problem is to consider an overall objective function that is the weighted sum of the single objective functions. This process is also known as *scalarization*.

1.1.3 Approach, method and technique

Figure 1.4 depicts the various approaches and methods that can be used to solve the trajectory optimization problem.
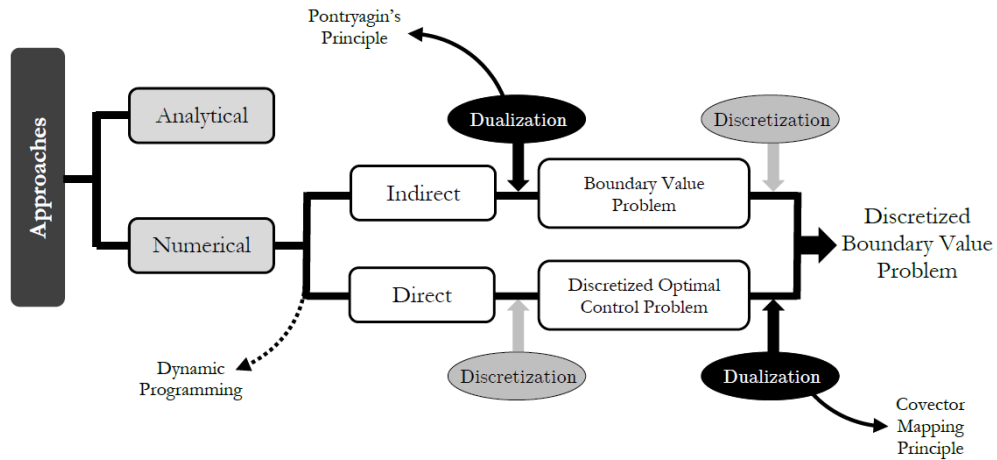
Figure 1.4: Taxonomy of approaches in spacecraft trajectory optimization [1]

After modeling the spacecraft dynamics and defining the objective function, it is necessary to choose an approach for finding the optimal trajectory. In general, *analytical* and *numerical approaches* can be exploited.

Analytical approaches are the most preferred since they often provide solutions directly based on mathematical representations with no approximation. However, due to the difficulty of the problem, they are achieved only in special cases (e.g. very low-thrust orbit raising).

Numerical approaches are increasingly advantageous as the model and problem complexity increase. The most popular methods within these approaches are:

- *Direct methods.* These methods are based on the concept of parameterization on state variables $\mathbf{x}(t)$ and control inputs $\mathbf{u}(t)$; the continuous optimal control problem is transcribed into a parameter optimization problem. The effect is to generate nonlinear constraint equations that must be satisfied by the parameters, which are the discrete representations of the state and control time histories [2]. Although direct methods are less accurate than indirect methods, they are more attractive due to their ease of implementation, greater domain of convergence, and reduced problem size.

- *Indirect methods* are those using the analytical necessary conditions from the calculus of variations. This requires the addition of costate variable (or adjoint variables) of the problem, equal in number to the state variables, and their governing equations [2]. While indirect approaches are often more accurate than direct methods, three major issues arise. First, there is the necessity

of deriving analytic formulations for the necessary conditions, which can be discouraging when working with complex problems. Second, the region of convergence may be quite small, as it is necessary to guess values for adjoint variables. Third, for problems with path inequalities, it is necessary to guess the sequence of constrained and unconstrained subarcs [5].

Figure 1.5 depicts the various techniques that can be used to solve the trajectory optimization problem.
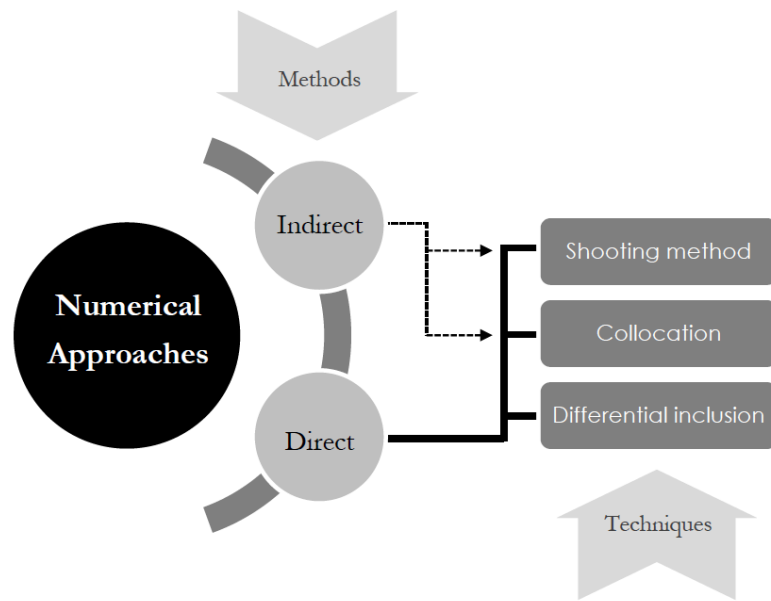
Figure 1.5: Methods and techniques in numerical approaches [1]

Except for the differential inclusions technique, which is a strictly direct method, the other techniques presented can be employed with both direct and indirect methods.

- By using the *Differential inclusions* technique, the equations of motion are enforced at each discrete time applying inequality constraints on state derivatives. The upper and lower bounds on the control vector are substituted into the equations of motion to obtain these inequality constraints. This technique removes the explicit dependence on control values at each node, but it can become numerically unstable and its formulation can be problem dependent [1].

- Shooting technique is an iterative strategy for calculating state histories given system control histories; this technique can define the problem in terms of a

relatively small number of optimization variables. This technique is appealing because the marching integration automatically enforces the equations of motion. Thus, by reducing the number of constraints that must be applied, the problem size is decreased.

- *Collocation* technique uses quadrature rules or interpolation to enforce the equations of motion. An interpolating function (interpolant) is solved in such a way that it passes through the state values while maintaining the state derivatives at the nodes spanning one time interval (or subinterval). The interpolant is then evaluated at collocation points, which are positions between nodes. An equality constraint is generated at each collocation point, equating the interpolant derivative to the state derivative function, ensuring that the equations of motion hold [1].

1.2   Problem statement and thesis objective

This thesis investigates the problem of trajectory optimization for the case of multiple Near-Earth Asteroid (NEAs) rendezvous missions, using Electric Propulsion (EP). The examined space mission, in particular, considers a spacecraft departing from Earth at t_0 and visiting N asteroids at different dates t_N, with at most $N = 3$. A rendezvous maneuver is carried out for each asteroid, with a stay of about two months; after that, the spacecraft will continue its journey to the next asteroid. Figure 1.6 depicts a typical three-target mission trajectory.

For what concern the problem mathematical modeling, the patched-conics approximation, which considers the two-body model, can be used to describe this interplanetary trajectory: the hypothesis of a point mass spacecraft under the influence of a single body, in this scenario the Sun, is thus assumed. Only the heliocentric legs are considered. Chapter 5 presents the adopted motion equations. The objective function for the analysed mission is the spacecraft final mass. Considering the Mayer formulation, it can be expressed as:

$$J = m_f \tag{1.3}$$

A numerical code that implements an indirect method using shooting techniques is employed to solve the trajectory optimization problem. As stated in the previous section, one of the major disadvantages of indirect methods is the requirement to start the procedure with a tentative solution that must be sufficiently close to the optimal one. Thus, the goal of this thesis is to propose appropriate procedures for overcoming convergence issues and finding low-cost optimized solutions to the analyzed problem.
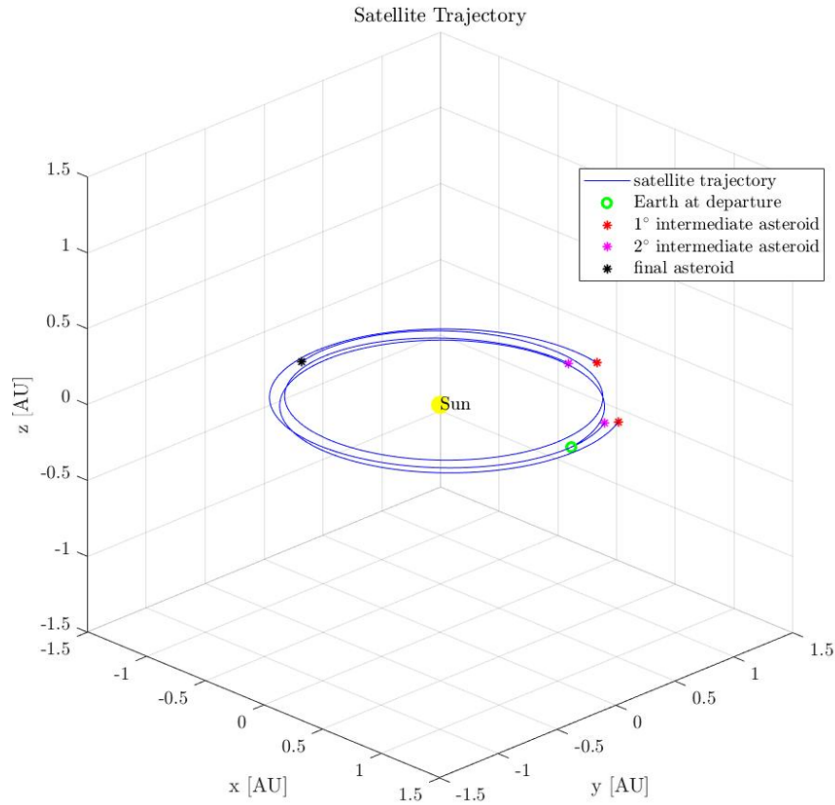
Figure 1.6: Multiple NEAs rendezvous mission example

1.3 Thesis overview

The thesis is organized as follows:

In Chapter 2 a brief overview of the mission's scientific objectives is provided. The primary motivations for the interest in Near-Earth Asteroids are discussed, as are the main properties of these celestial bodies.

Chapter 3 introduces the mathematical modelling of the system's dynamics. In section 3.1 the basic theory of orbital mechanics is presented. A focus on the two-body model is given, since it is adopted in this work. Section 3.2 discusses the basics of space propulsion. A global overview of propulsion systems is offered, followed by a review of electrical thrusters, that are considered for the examined missions.

Chapter 4 covers the global properties and mathematical aspects of the indirect

method used to optimize space trajectories. General notions of the *Optimal Control Theory* are explained, since it represents the basis of indirect methods. After that, a description of the resulting Boundary Value Problem is provided.

In chapter 5 the preceding Chapter's concepts and generic equations are applied to the analysed missions. Furthermore, reference parameters are provided to formulate the problem in a dimensionless form. Finally a set of appropriate boundary conditions is provided.

In chapter 6 the methodology for addressing the investigated problem is proposed. In particular, suitable procedures to define tentative solutions and then to find multiple optimized rendezvous missions are described.

The obtained results for missions to one, two, and three targets are presented in Chapter 7, in order to validate the proposed procedures for defining initial guesses. A summary of solutions is also provided.

Conclusions and possible future advances of this work are provided in Chapter 8.

Chapter 2

Mission's scientific objectives

As mentioned, this thesis investigates the problem of trajectory optimization for the case of multiple Near-Earth Asteroids rendezvous missions. In this Chapter will be thus presented the characteristics of these celestial bodies as well as the main drivers behind the interest in NEAs.

2.1 Near-Earth Objects

Near-Earth Objects (NEOs) are comets and asteroids that have been nudged by the gravitational attraction of nearby planets into orbits that allow them to enter the Earth's neighborhood. In terms of orbital elements, NEOs have a perihelion distance q (the orbit's closest approach to the Sun) less than 1.3 AU (1 AU, an "Astronomical Unit", is the mean distance between the Earth and the Sun, around 150 million km).

Composed mostly of water ice with embedded dust particles, comets originally formed in the cold outer planetary system, while most of the rocky asteroids formed in the warmer inner solar system, between the orbits of Mars and Jupiter. The scientific interest in comets and asteroids is due largely to their status as the relatively unchanged remnant debris from the solar system formation process some 4.6 billion years ago [6]. They contain information that has been lost in the planets through large-scale, planetary processes such as accretion, tectonism, volcanism, and metamorphism. Knowledge of the asteroids and comets as less processed material from the early solar nebula, studied together with direct samples in the form of meteorites, is critical to piecing together a scenario for the formation of the solar system [7].

The vast majority of NEOs are asteroids, referred to as Near-Earth Asteroids (NEAs).

2.1.1 Near-Earth Asteroids

Near-Earth Asteroids constitute the majority of the Near-Earth Objects population. Thanks to the operation of wide-field high sensitivity automated sky surveys the number of known NEAs is rapidly growing [8]. The following chart (Figure 2.1) shows the cumulative number of known Near-Earth Asteroids versus time. Totals are shown for NEAs of all sizes, those NEAs larger than $\sim 140\,m$ in size, and those larger than $\sim 1\,km$ in size [9]. It also reveals that most of the large NEAs (diameter $> 1\,km$) have already been detected, and therefore smaller object dominate the present discoveries.
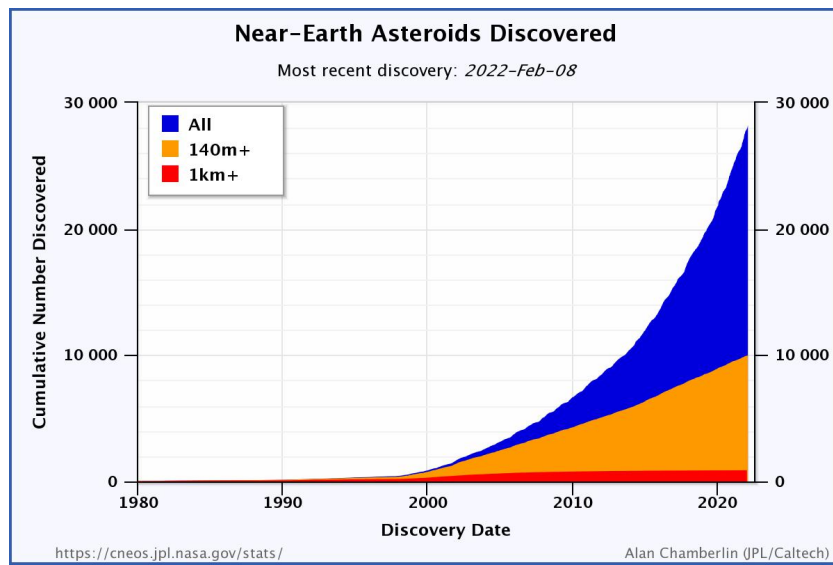
Figure 2.1: Cumulative number of known Near-Earth Asteroids [9]

NEAs are divided into four groups according to their perihelion distance, aphelion distance and their semi-major axes:

- *Amors* are Earth-approaching NEAs with orbits exterior to Earth's but interior to Mars';

- *Apollos* are Earth-crossing NEAs with semi-major axes larger than Earth's;

- *Atens* are Earth-crossing NEAs with semi-major axes smaller than Earth's;

- *Atiras* are NEAs whose orbits are contained entirely with the orbit of the Earth.

There are three main drivers behind the interest in NEAs:

- **expected scientific return**.

  - Scientists can glean information about the formation of the Solar System by studying their composition and structure.
    Furthermore, since some of these objects may collide with the Earth, asteroids are also important for having significantly modified the Earth's biosphere in the past. During the early solar system, the carbon-based molecules and volatile materials that served as the building blocks of life may have been brought to the Earth via asteroid and comet impacts.

  - Most of NEAs have peculiar orbits that scientists study to reveal orbital change processes. Most of them appear to have originated from the main asteroid belt through a combination of processes, including planetary perturbations, collisions, thermal forces, and solar wind pressure. Dynamicists have simulated the pathways that objects might take from unstable regions of the Asteroid Belt using computations of dynamical forces acting in the solar system. In some cases, fragments from asteroid collisions may be violently cast into these regions of instability. However, a softer touch may play an even bigger role. Constant warming by the Sun causes asteroids of all sizes to reradiate their heat back into space. Because the asteroids are rotating, the reradiation does not occur in the same direction as the incoming sunlight, resulting in a small force acting on the asteroid. This force acts as a very gentle push on the asteroid, which over many millions of years can cause the asteroid to slowly drift inward or outward from its original main-belt location. This is called Yarkovsky drift and is especially effective on small objects (Figure 2.2).
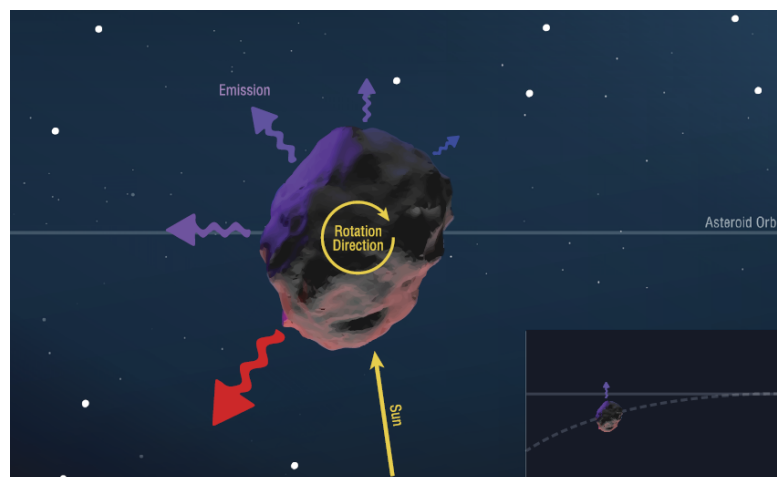
Figure 2.2: The Yarkovsky Effect [10]

- **Planetary defense**. In addition to originating life, NEAs could also destroy it. It is evident that a ten-kilometer-wide impactor caused the Cretaceous-Paleocene extinction event, when it made the Chicxulub crater over 64 million years ago. More recently, the Chelyabinsk bolide in February 2013, which caused massive property damage and injured around 1500 people, was only 20 m wide, weighed 12,000 metric tons, and entered our atmosphere at a relative speed of 19 km/s.
  Potentially Hazardous Asteroids (PHAs) are currently defined based on parameters that measure the asteroid's potential to make threatening close approaches to the Earth. Specifically, all asteroids with an Earth Minimum Orbit Intersection Distance (MOID) of 0.05 AU or less and an absolute magnitude (H) of 22.0 or less (larger than about 140 m in diameter) are considered PHAs. Understanding of the physical properties of these threatening objects and their response to a mitigation action are the first steps to design an efficient mitigation strategy.

- **Mining**. As a matter of fact, asteroids offer a source of volatiles and an extraordinarily rich supply of minerals that can be exploited for the exploration and colonization of our solar system. [6, 7, 11, 12]

For all these reasons, in the last decades, near-Earth asteroids received considerable attention which in turn stimulated the interest in their exploration. Indeed, close-up observations of these objects will drastically increase our knowledge about the overall NEA population. Moreover, near-Earth asteroids' proximity to the Earth makes transfers to these bodies relatively low-cost in terms of ΔV and propellant consumption. The population of known NEAs is already quite large and continuously grows due to the discovery of new objects. The existence of such a large set of possible targets provides many opportunities for scientific missions to new objects, in addition to ones already reached. Hence, a multiple NEA rendezvous mission can help the scientific community to improve our knowledge about these objects.

Chapter 3

Mathematical modelling of the problem

As the first step of facing the spacecraft trajectory optimization problem, the dynamics of the spacecraft need to be mathematically modeled. The spacecraft trajectory model can be referred to a set of ordinary differential equations representing the time history of position and velocity of the spacecraft [4]. Fundamentals of Astrodynamics and Space Propulsion are presented below to make clear the mathematical formalization of the problem.

3.1 Fundamentals of Astrodynamics

The basic theory of orbital mechanics is presented in this section. In particular, the two-body and N-body equations of motion are introduced. Orbit determination through the classical orbital elements and coordinate transformations are then explained. A focus on Kepler's equation is also presented. Finally, an overview of interplanetary missions is given with the description of the patched-conics theory. The following section's theoretical principles are primarily based on [13] and [14].

3.1.1 Newton's Law of Universal Gravitation

Sir Isaac Newton was the first scientist to specifically articulate the concept of gravitational force, and his writings detailed how gravitational attraction affects both falling objects and the motions of celestial bodies. However, Newton piggybacked on the observations and theories of other mathematicians and physicists, including: Max Kepler, Robert Hooke, Edmund Halley, and Christopher Wren. Besides enunciating his three laws of motion in the *Principia*, he formulated the law of gravity by stating that any two bodies attract one another with a force

proportional to the product of their masses and inversely proportional to the square of the distance between them:

$$\mathbf{F}_g = -\frac{GMm}{r^2}\frac{\mathbf{r}}{r} \qquad (3.1)$$

where $\mathbf{F}_g$ is the force on mass m due to mass M and $\mathbf{r}$ is the vector from M to m. The universal gravitational constant, G, has the value $6.6742 \times 10^{11}\, m^3/kg \cdot s^2$.
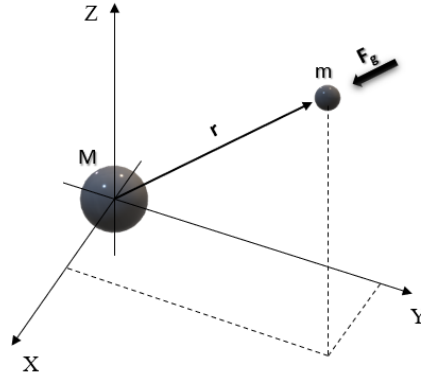
Figure 3.1: Newton's Law of Gravity

3.1.2 The N-body problem

By applying Newton's law of universal gravitation it is possible to examine the motion of a body, like an Earth satellite or an interplanetary probe. At any given time in their journey, these objects are being acted upon by several gravitational masses and may even be experiencing other forces such as drag, thrust, and solar radiation pressure.

We assume a system of n-bodies $(m_1, m_2, m_3, \dots, m_n)$ within an inertial reference frame XYZ, illustrated in figure 3.2, one of which is the body whose motion we wish to study, the ith body, m_i. For the sake of simplicity, the following hypothesis are considered:

- spherical symmetry of the mass distribution;

- homogeneity of the mass distribution;

- punctiform masses concentrated in the bodies' centers;

- only gravitational interaction among the bodies, neglecting other external or internal forces acting on the system.

16
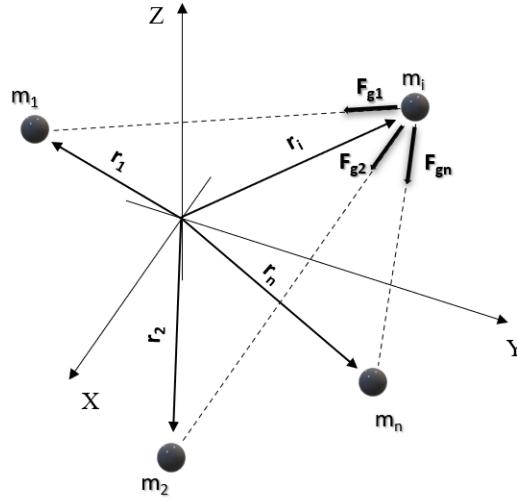
Figure 3.2: The N-Body Problem

Applying Newton's law of universal gravitation to this system, the force $\mathbf{F}_{gn}$ exerted on m_i by m_n can be expressed as

$$\mathbf{F}_{gn} = -\frac{Gm_i m_n}{r_{ni}^2}\frac{\mathbf{r_{ni}}}{r_{ni}} \tag{3.2}$$

where

$$\mathbf{r_{ni}} = \mathbf{r_i} - \mathbf{r_n}$$

Thus, the vector sum, $\mathbf{F}_g$ of all the gravitational forces acting on the ith body is

$$\mathbf{F}_g = -Gm_i \sum_{j=1, j\neq i}^{n} \frac{m_j}{rji^2}\frac{\mathbf{r_{ij}}}{r_{ij}} \tag{3.3}$$

and its equation of motion is

$$\mathbf{\ddot{r}_i} = -G \sum_{j=1, j\neq i}^{n} \frac{m_j}{rji^2}\frac{\mathbf{r_{ij}}}{r_{ij}} \tag{3.4}$$

Equation (3.4) holds for $1 \leq i \leq n$, so it is a system of n second order autonomous vector differential equations, for which numerical integration is needed.

3.1.3 The two-body problem

The motion of a satellite about the Earth is governed primarily by the attraction between Earth and satellite. This is also true for satellites at an altitude of some ten thousand kilometers. The effects of the gravitation attraction of the Sun, Moon,

and planets are very small. If at a first approximation, we completely neglect these effects, we deal with a two-body problem. Unlike the N-body problem, the two-body problem can be solved analytically, and since its solution is near to physical reality, it constitutes the basic algebra of celestial mechanics.

In this model, the motion of the body i^{th} is considered to be determined uniquely by the mutual attraction with the body k^{th}. Considering a non-rotating reference frame with its origin at body k^{th}, the motion of the body i^{th} is described by:

$$\ddot{\mathbf{r}} = -\frac{\mu}{r^2}\frac{\mathbf{r}}{r} \tag{3.5}$$

where

$$\mu = G\left(m_k + m_i\right)$$

and $\mathbf{r}$ is the position vector of body i^{th}.

In many cases, however, such as the motion of planets about the Sun or the motion of satellites about the Earth, we deal with problems where $m_k \gg m_i$. Then, we can safely approximate μ by

$$\mu = Gm_k\,.$$

In this case the problem is defined as the *Restricted Two-Body Problem*, and μ is called *gravitational parameter* or *attraction parameter* of body k^{th}.

Values of μ for each major attracting body are listed in table 3.1.

Gravitational Parameter of Sun $[km^3 s^{-2}]$	$\mu_{\odot}$	1327.1244×10^8
Gravitational Parameter of Earth $[km^3 s^{-2}]$	$\mu_{\oplus}$	3986.0043×10^2
Gravitational Parameter of Moon $[km^3 s^{-2}]$	$\mu_{\mathbb{C}}$	4902.8001
Gravitational Parameter of Mars system $[km^3 s^{-2}]$	$\mu_{\mars}$	42828.3758
Gravitational Parameter of Jupiter system $[km^3 s^{-2}]$	$\mu_{\jupiter}$	1267.1276×10^5

Table 3.1: Gravitational Parameter of major attracting bodies

3.1.4   Constants of the motion

The gravitational field is conservative. This means that an object, moving under the influence of gravity alone does not lose or gain mechanical energy, but only exchanges one form of energy, kinetic, for another, potential.

Furthermore, because this force is always applied radially toward the center of the large mass, we would predict the satellite's angular momentum about the center of our reference frame to remain constant.

18

Conservation of Mechanical Energy

Dot multiplying equation (3.5) by $\dot{\mathbf{r}}$:

$$\dot{\mathbf{r}} \cdot \ddot{\mathbf{r}} + \dot{\mathbf{r}} \cdot \frac{\mu}{r^2} \frac{\mathbf{r}}{r} = 0$$

which leads to the following expression:

$$\frac{\mathrm{d}}{\mathrm{d}t} \left(\frac{v^2}{2} - \frac{\mu}{r} \right) = 0$$

As a consequence of this formalization, it is possible to conclude that the *specific mechanical energy E* of a satellite, which is the sum of its kinetic energy per unit mass and potential energy per unit mass, remains constant during its orbit, neither increasing nor decreasing as a result of its motion. The expression for E is:

$$E = \frac{v^2}{2} - \frac{\mu}{r} \tag{3.6}$$

Conservation of Angular Momentum

Cross multiplying equation (3.5) by $\mathbf{r}$:

$$\mathbf{r} \times \ddot{\mathbf{r}} + \mathbf{r} \times \frac{\mu}{r^2} \frac{\mathbf{r}}{r} = 0$$

where the second term vanishes and the first one can be written as:

$$\frac{\mathrm{d}}{\mathrm{d}t} \left(\mathbf{r} \times \mathbf{v} \right).$$

The expression $\mathbf{r} \times \mathbf{v}$ is the vector $\mathbf{h}$, called *specific angular momentum*. Therefore, for a satellite

$$\mathbf{h} = \mathbf{r} \times \mathbf{v} \tag{3.7}$$

remains constant along its orbit. For this reason, the satellite's motion must be confined to a plane which is fixed in space, the *orbital plane*.

3.1.5 The trajectory equation

A partial solution to the equation (3.5) which tell us the size and shape of the orbit is easy to obtain. Crossing this equation into $\mathbf{h}$ leads toward a form which can be intagrated, and solving for r it is possible to obtain the trajectory equation:

$$r = \frac{\frac{h^2}{\mu}}{1 + \left(\frac{B}{\mu} \right) \cos \nu} \tag{3.8}$$

where B is the absolute value of the vector constant of integration, and ν is the angle between the constant vector and the radius vector.

This equation has the same mathematical form as the generic equation of a conic section written in polar coordinates with the origin at a focus, and where ν is the angle between **r** and the point on the conic nearest the focus:

$$r = \frac{p}{1 + e \cos \nu} \tag{3.9}$$

In this equation p is called *semi-latus rectum* and e is called the *eccentricity*. The eccentricity determines the type of conic section represented by equation (3.9):

$e = 0$	Circle
$1 < e < 0$	Ellipse
$e = 1$	Parabola
$e > 1$	Hyperbola
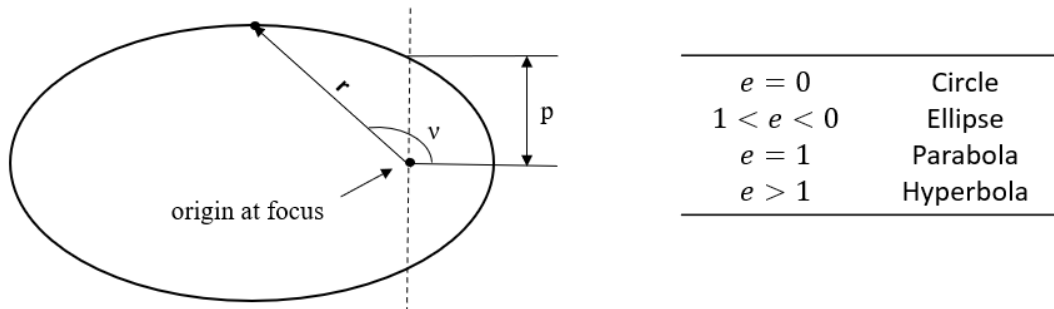
Figure 3.3: General equation of conic sections in polar coordinates [13]

Thus, the family of these curves represent the only possible path for an orbiting object in the two-body problem.

3.1.6 Classical Orbital Elements

Five independent quantities are sufficient to completely describe the size, shape and orientation of an orbit. To pinpoint the position of the satellite along the orbit at a particular time, a sixth element is required. Therefore, the classical set of six orbital elements are defined as follows:

1. a, *semi-major axis*, a constant defining the size of the conic orbit. This orbital element is directly connected to the energy of the orbit, which can be also expressed as:

$$E = -\frac{\mu}{2a} \tag{3.10}$$

   This relationship, which is valid for all conic orbits, tells us that the semi-major axis of an orbit depends only on the specific mechanical energy of the satellite. Circle and ellipse show a positive a, while for the parabola a is infinite and the hyperbola a is negative. This implies that that the specific mechanical energy

of a satellite in a closed orbit is negative, while E is zero on a parabolic orbit and it is positive on a hyperbolic orbit.

2. *e, eccentricity*, as previously seen, a constant defining the shape of the conic orbit.

3. *i, inclination*, the angle between the unit vector of the Z axis and the angular momentum vector **h**.

4. Ω, *longitude of the ascending node*, the angle, in the reference plane, between the unit vector of X axis and the point where the satellites crosses through the reference plane in a northerly direction (ascending node) measured counterclockwise when viewed from the north side of the reference plane.

5. ω, *argument of periapsis*, the angle, in the orbital plane, between the ascending node and the periapsis point, measured in the direction of the satellite's motion.

6. ν, *true anomaly* at epoch t, the angle, in the orbital plane, between the periapsis point and satellite.
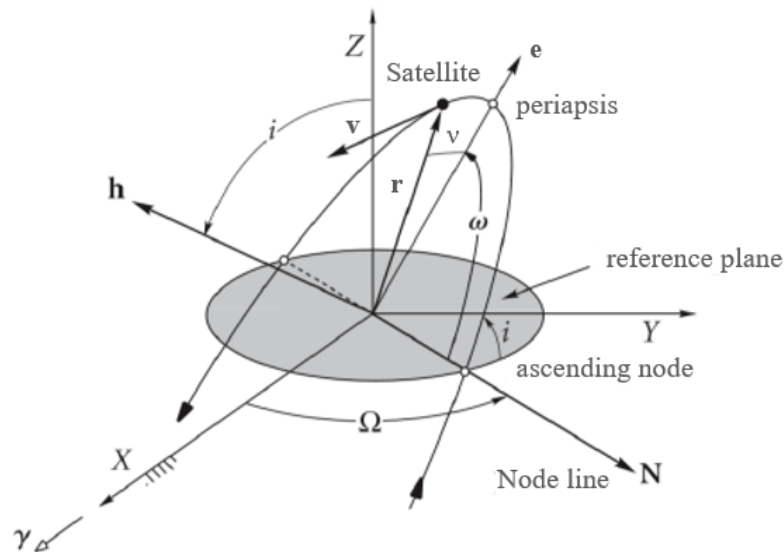
Figure 3.4: Orbital Elements [14]

3.1.7 Kepler's Equation

Equation (3.9) gives the position of the satellite in its orbit as a function of the *true anomaly*. For many practical reasons, it is necessary to determine the position

of satellite as a function of time.

The absolute value of the specific angular momentum is:

$$h = r v_{\perp} = r^2 \dot{\nu} \tag{3.11}$$

Starting from the latter equivalence and considering equation (3.9), it is possible to write:

$$\frac{\mathrm{d}\nu}{\mathrm{d}t} = \frac{h}{r^2} = \sqrt{\frac{\mu}{p^3}} \left(1 + e \cos \nu\right)^2$$

From this equation:

$$\Delta t = \sqrt{\frac{p^3}{\mu}} \int_{\nu_0}^{\nu_e} \frac{\mathrm{d}\nu}{\left(1 + e \cos \nu\right)^2} \tag{3.12}$$

where Δt is the time interval in which the body's true anomaly increases from ν_0 to ν_e. The integral in equation (3.12) can be evaluated for elliptic, parabolic and hyperbolic orbits. The resulting expressions are however cumbersome if the orbit is an ellipse or a hyperbola.

Considering the elliptic orbit, the concept of *eccentric anomaly E* is then introduced, defined such that the equation of the elliptic trajectory can be written as:

$$r = a \left(1 - \cos E\right)$$

The angle E can be constructed by using an auxiliary circle, as is shown in Figure 3.5.
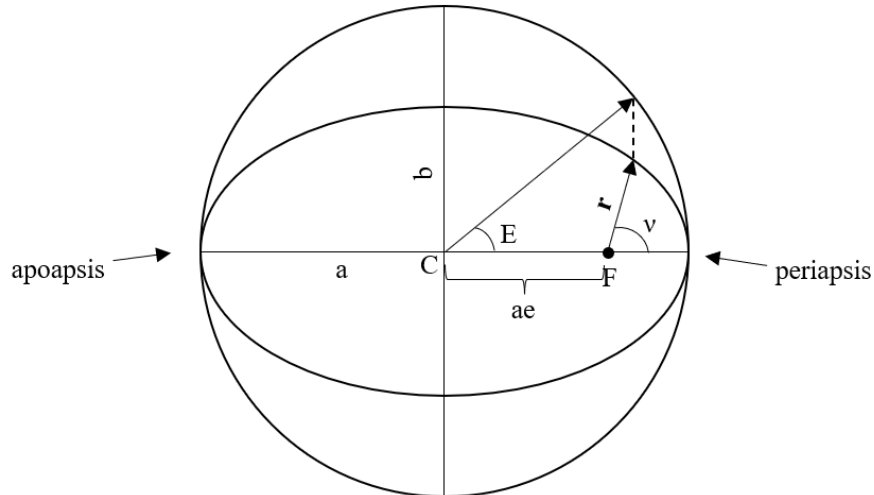
Figure 3.5: The eccentric anomaly

The introduction of this quantity leads to the following expression:

$$E - e \sin E = \sqrt{\frac{\mu}{a^3}} \, (t - \tau) \tag{3.13}$$

where τ is a constant of integration which represents the *time of periapsis passage.* The term on the right side of the equation is defined as the *mean anomaly*

$$M = n \, (t - \tau)$$

where

$$n = \sqrt{\frac{\mu}{a^3}}$$

Thus, equation (3.13) can be written in the form

$$E - e \sin E = M \tag{3.14}$$

Equation (3.14) is known as *Kepler's Equation.* It relates position, through the angle E, to time elapsed after the periapsis passage. In particular, to calculate where the body is at a given time, this equation have to be solved with a numerical iteration method. Ones E is known, then it is possible to evaluate the position of the body along its orbit.

3.1.8 Interplanetary Missions

In order to study missions toward Near-Earth Asteroids, it is necessary to introduce some basic notions about interplanetary transfers. These are studied under the hypothesis of the *patched conics* method. The mission can be divided into three phases:

- *Escape* from the sphere of influence of the departure body;

- *Heliocentric Transfer Orbit*;

- *Arrival* in the sphere of influence of the target body.

The sphere of influence (SOI) is the spherical region around the celestial body where the primary gravitational influence on an orbiting object is that body. This is usually used to describe the areas in our solar system where planets dominate the orbits of surrounding objects (such as moons) despite the presence of the much more massive Sun. In a more general sense, the patched conic approximation is only valid within the SOI.

The general equation describing the radius of the sphere of influence, r_{SOI} of a planet in the solar system is:

$$r_{SOI} = D \left(\frac{m_p}{m_\odot} \right)^{\frac{2}{5}} \tag{3.15}$$

where D is the planet's distance relative to the Sun, m_p and m_s are the masses of the planet and Sun, respectively.

In the patched conic approximation, once an object leaves the planet's SOI, the only gravitational influence is the Sun, until the object enters another body's SOI. The radius of the Earth's sphere of influence is $\simeq 10^6$ km; this dimension, if compared to the extension of the solar system, is negligible.

This thesis does not cover the departure and arrival phases. The only point of interest is the heliocentric transfer. The spacecraft leaves the Earth sphere of influence at the initial time with position and velocity coincident with the planet's value. At rendezvous with the target at the final time, position and velocity match the asteroid's values.

3.2 Fundamentals of Space propulsion

The basic concepts of space propulsion are given in this section. A global overview of the ideas shared by all propulsive systems is provided, followed by an examination of electrical thrusters, which are being considered for the investigated missions. As previously stated, if no external force is applied to a body in space, its trajectory is a conic section that is totally determined by the body's position and velocity at a given moment. The propulsion system can provide a force that modifies the velocity of the spacecraft, thereby preserving, or altering the trajectory.

3.2.1 Generalities

The theory of propulsion is founded on the "action-reaction" concept, which states that whenever one object exerts a force on another, the second object exerts an equal and opposite force on the first.
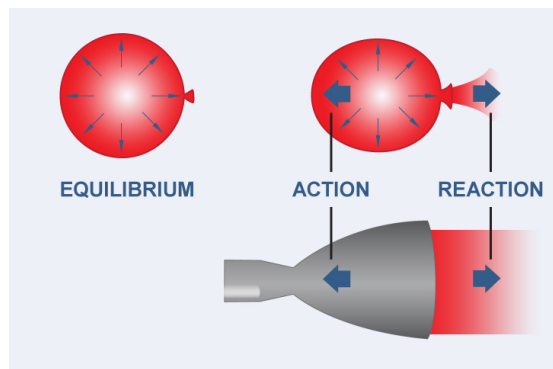
Figure 3.6: Action and reaction principle [15]

As a result, carrying onboard something to exchange momentum with is the most straightforward way to generate thrust in space: thus, propellant is required.

Because all propulsors use the action-reaction principle, it is possible to explain their behavior in general and introduce some especially significant parameters by means of a simplified model.

The isolated system in figure 3.7 is used to introduce these concepts. Aligned velocity vectors are assumed. By definition, this system is not subjected to any external forces.
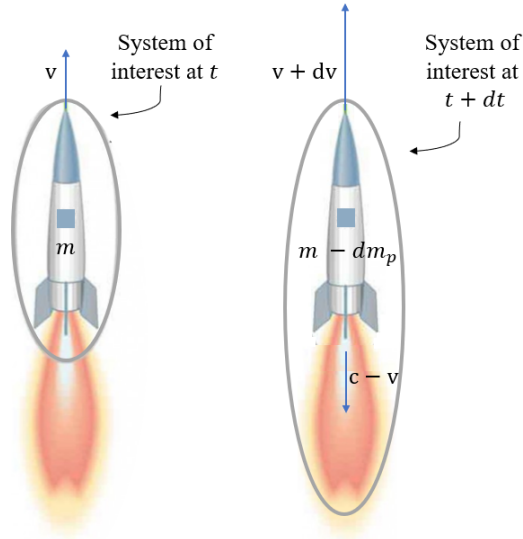
Figure 3.7: Momentum conservation scheme

The system of interest is depicted as a rocket accelerating straight up. On the left side, at time t, the rocket has a mass m and a velocity v relative to Earth, and hence a momentum mv. On the right, an infinitesimal interval of time dt has elapsed during which the rocket ejected a portion of its mass, the propellant mass dm_p. However, the remaining mass $(m - dm_p)$ has a higher velocity $(v + dv)$. The velocity increase dv is proportional to the velocity at which the propellant mass is discharged. The velocity of the propellant mass relative to the rocket can be expressed as the *effective discharge velocity c*.

However, this is not the actual exit velocity of the propellant mass. This is due to the fact that when the propellant is accelerated in the nozzle, it is subjected to pressure forces as well. At the nozzle exit section, the portion of propellant that is still inside the system exchanges indeed a pressure force with the part of propellant that is already outside. The magnitude of this force, known as static thrust, is determined by the difference between the exit pressure and the ambient pressure. Anyway, this term is negligible in space propulsion, and c can be approximated as the propellant exit velocity.

Thus, the absolute propellant mass velocity can be expressed as $c - v$.

Within an isolated system, momentum conservation holds true. As a result, the following relationship may be written:

$$mv = (m - \mathrm{d}m_p)(v + \mathrm{d}v) - \mathrm{d}m_p(c - v)$$

which, neglecting the second degree infinitesimal terms and introducing the propellant flow $\dot{m}_p$, becomes:

$$m\,\frac{\mathrm{d}v}{\mathrm{d}t} = c\,\dot{m}_p$$

According to Newton's second law of motion, since the term on the left is the product of the body's mass and acceleration, the term on the right must be the force applied to the body itself, the *thrust*:

$$T = \dot{m}_p\,c \tag{3.16}$$

Thus, the amount of power required to accelerate the propellant at the velocity that produces a thrust of intensity T, known as *thrust power*, is:

$$P_T = \frac{1}{2}\,T\,c = \frac{1}{2}\,\dot{m}_p\,c \tag{3.17}$$

Thrust is one of the most crucial propulsion's performance parameters. Its integral over a complete mission is called the *total impulse*

$$I_t = \int_{t_0}^{t_f} T\,\mathrm{d}t \tag{3.18}$$

The total impulse per unit weight of the propellant is the *specific impulse*, I_{sp}:

$$I_{sp} = \frac{I_t}{m_p g_0} \tag{3.19}$$

where m_p is the total propellant mass and g_0 is the gravitational acceleration on the Earth's surface. The specific impulse shows how much impulse can be obtained from a unit weight of propellant, and as one tries to keep weights as low as possible, it is evident that a high specific impulse is desirable. The specific impulse may also be interpreted as the time during which a propellant can deliver a force which equals the propellant's initial weights [16].

If T and c are constants, the specific impulse can be expressed as:

$$I_{sp} = \frac{c}{g_0} \tag{3.20}$$

Thus, neglecting the constant parameter g_0, the values of c and I_{sp} are identical. In fact, both the specific impulse and the effective discharge velocity indicate how

26

efficiently the propellant is used to generate thrust.

The space mission's propulsive cost can be calculated using the total impulse as well as the *characteristic velocity* ΔV. The latter parameter represents the ideal (because no losses or external disturbances are considered) variation of the body's velocity across the manoeuvres. It can be defined as:

$$\Delta V = \int_{t_0}^{t_f} \frac{T}{m} \, \mathrm{d}t \tag{3.21}$$

Substituting Equation (3.16) and considering that

$$\dot{m}_p = -\frac{\mathrm{d}m}{\mathrm{d}t}$$

Equation (3.21) can be rewritten as:

$$\Delta V = \int_{m_f}^{m_0} \frac{c}{m} \, \mathrm{d}m$$

If the effective discharge velocity is constant, the *Tsiolkovsky* equation (or *Rocket* equation) can be derived in its two formulations:

$$\Delta V = c \ln \frac{m_0}{m_f} \qquad \Longleftrightarrow \qquad m_f = m_0 e^{-\frac{\Delta V}{c}} \tag{3.22}$$

The Tsiolkovsky equation relates the propulsive cost and the propellant mass required to complete the mission. Because propellant consumption and propulsive effort are linked by an exponential relationship, having an effective discharge velocity that is at least similar to the ΔV is crucial. In fact, if the specific impulse is too low, the final mass is negligible in comparison to the initial mass, and hence no payload can be carried, as showed in Figure 3.8.

Rocket Equation Results

$\Delta V/c$	m_f/m_i	m_i/m_f
5	0.0067	148
2	0.135	7.39
1	0.368	2.72
0.5	0.606	1.65
0.2	0.819	1.22
0.1	0.905	1.11

Figure 3.8: Rocket equation results for different $\Delta V/c$ ratios [17]

As a result, a large specific impulse is required. The higher c, the less propellant is required to complete the maneuver.

3.2.2 Electric Propulsion

Figure 3.9 presents typical characteristic velocity values for several space missions.

Typical Characteristic Velocities

Mission	ΔV, km/s
LEO insertion	10
1 year station keeping	0.5
LEO-GEO (impulsive)	3.5
LEO-GEO (spiral)	6
Earth escape (impulsive)	3.2
Earth escape (spiral)	8
Earth-Mars (impulsive)	5.5
Earth-Mars (spiral)	6
Earth-Jupiter (spiral)	16.7
Earth-Alpha Centauri	30000

Figure 3.9: Typical Characteristic Velocities [17]

To achieve the desired effective discharge velocities, processes different from the simple heating of a propellant stream by chemical reaction or by solid element heat transfer must be employed; for instance, high enthalpy heating of an insulated gas stream or direct acceleration of it by applied body forces are viable techniques for achieving the needed *c*. Either process is most reasonably accomplished by electrical means [18].

Electric Propulsion can be thus defined as the "acceleration of gases by electrical heating and/or by electric and magnetic forces" [18]. This definition can be distinct into three concepts:

- *Electrothermal propulsion*, where the propellant is heated using electrical power and then expanded in a suitable nozzle. Thus thrust is produced converting thermal energy into kinetic energy.

- *Electrostatic propulsion*, where the propellant is ionized and accelerated by direct application of electric body forces. In particular, the ions are accelerated through an electric field and the exit beam is neutralized.

- *Electromagnetic propulsion* where a ionized propellant stream is accelerated by interactions of external and internal magnetic fields with electric currents driven through the stream.

These mechanisms result more than adequate to qualify for the large velocity increment space missions outlined in Figure 3.9.

Regardless of the physical method used to accelerate the propellant, all electrical thrusters exhibit some common characteristics. In fact, they all transform electrical power into thrust. This conversion process presents a specific global efficiency that changes depending on the thruster category under consideration. Mathematically, this can expressed as:

$$\eta P_E = \frac{1}{2} T c \tag{3.23}$$

where η is the global efficiency and P_E is the electric power consumption.
This relationship can be inverted to express the effective discharge velocity:

$$c = \frac{2\eta P_E}{T}$$

Thus, in case of electric propulsion systems, it is possible to raise c (within the constraints given by present technologies) while accepting low thrust or large power source's mass. When compared to chemical rockets, electrical thrusters have indeed a higher specific impulse and a lower thrust. Figure 3.10 shows typical thrust and specific impulse values for both chemical and electric propulsion.

Characteristics of Propulsion Systems

System	Specific Impulse, s	Thrust, N
Liquid monopropellant (CP)	200-250	0.01-100
Liquid bipropellant (CP)	300-450	$0.01\text{-}10^7$
Solid propellant (CP)	200-300	$1\text{-}10^6$
Hybrid propellant (CP)	250-350	$1\text{-}10^6$
Resistojets (EP)	200-350	0.2-0.3
Arcjets (EP)	400-1000	0.2-1
Ion thrusters (EP)	2000-5000	<0.2
Hall thrusters (EP)	1500-2000	<2
Pulsed plasma thrusters (EP)	600-2000	<0.01
MPD thrusters (EP)	2000-5000	<2

Figure 3.10: Characteristics of Propulsion systems[17]

As mentioned, electrical thusters have low thrusts ($10\,\mu\text{N} - 1\text{N}$) but high specific impulse values ($200 - 5000$). Given these features, electric propulsion is ideal for long and efficient missions like the ones examined in this thesis

Chapter 4

Indirect Optimization of Spacecraft Trajectories

Global properties and mathematical aspects of the indirect method exploited to optimize space trajectories are presented in this chapter.

As mentioned in Chapter 1, the spacecraft trajectory optimization problem can be defined as the identification of a trajectory that maximizes or minimizes a significant quantity. Given the relevance of propellant consumption, which has a significant impact on the mission's cost and feasibility, the most common goal is to minimize it, or equivalently to maximize the fraction of the spacecraft that is not devoted to it.

Analytical solutions for the optimal trajectory can be obtained in special cases; as a result, significant solutions must be found through the use of approximated theories or numerical approaches. The majority of numerical techniques for optimizing spacecraft trajectories may be divided into three categories:

- Direct methods;

- Indirect methods;

- Evolutionary algorithms.

This chapter focuses on indirect methods, which provide useful theoretical information about the problem which is dealt with, while also allowing for exact optimization, within the dynamical model's limitations and the precision of numerical integration. Because indirect methods are based on the *Optimal Control Theory*, this theory's general concepts will be discussed. Then, a description of the derived Boundary Value Problem is presented.

The following chapter's theoretical principles are primarily based on the research of professors Casalino [19] and Colasurdo [5].

4.1 Optimal Control Theory

The optimal control theory (OCT), which is based on calculus of variations, is used in the indirect approach to optimization.
A set of state variables $\mathbf{x}$ describes the system, and differential equations govern the evolution from the initial to the final state:

$$\frac{\mathrm{d}\mathbf{x}}{\mathrm{d}t} = \mathbf{f}(\mathbf{x}, \mathbf{u}, t) \tag{4.1}$$

These differential equations depend on:

- $\mathbf{x}$: state variables vector;

- $\mathbf{u}$: control variables vector;

- t: indipendent variable, time.

Considering the analysed case, it is convenient to divide the trajectory between the initial and final point (*external boundaries*) into n sub-intervals, which are defined as arches. The variables are continuous within each arch, but there may be discontinuities at the arches' interfaces (*internal boundaries*). The jth arc begins at t_{j-1_+} and finishes at t_{j_-}, with respectively $\mathbf{x}_{j-1_+}$ and $\mathbf{x}_{j_-}$ as state variables ($j-$ and $j+$ indicate values just before and after point j).
In general, the boundary conditions are both mixed and non-linear. As a result, nonlinear relations between state and temporal variables at the external and internal boundaries are involved.These constraints are collected into a vector χ, which is expressed as:

$$\chi\left(\mathbf{x}_{(j-1)_+}, \mathbf{x}_{j_-}, t_{(j-1)_+}, t_{j_-}\right) = 0 \qquad j = 1, \ldots, n \tag{4.2}$$

As steted in Chapter 1 the optimal problem can be defined as the search for the extremal values (minima or maxima) of the cost function J. Its general form is:

$$J = \varphi\left(\mathbf{x}_{(j-1)_+}, \mathbf{x}_{j_-}, t_{(j-1)_+}, t_{j_-}\right) + \sum_j \int_{t_{(j-1)_+}}^{t_{j_-}} \Phi(\mathbf{x}(t), \mathbf{u}(t), t) \, \mathrm{d}t \quad j = 1, \ldots, n \tag{4.3}$$

where

- φ is a function of state variables' and time's values at internal and external boundaries;

- integral of Φ, which is a function of state variables', control variables' and time's values at each instant.

It is worth noting that the functional J can be rewritten in either the *Lagrange* formulation ($\varphi = 0$) or the Mayer formulation ($\Phi = 0$). To define the optimization problem in this thesis, Meyer formulation is employed.

The functional can then be reformulated by including *Lagrange multipliers* $\boldsymbol{\mu}$ (constants associated with boundary conditions) and *adjoint variables* $\boldsymbol{\lambda}$ (associated with the differential equations). The modified functional J^* can be written as:

$$J^* = \varphi + \boldsymbol{\mu}^T \boldsymbol{\chi} + \sum_j \int_{t_{(j-1)_+}}^{t_{j-}} \boldsymbol{\lambda}^T (\mathbf{f} - \dot{\mathbf{x}}) \, \mathrm{d}t \tag{4.4}$$

J and J^* must clearly coincide if boundary constraints and state equations are satisfied. It is possible to differentiate J^* and obtain its first variation:

$$
\begin{aligned}
\delta J^* = {} & \left(-H_{(j-1)_+} + \frac{\partial \varphi}{\partial t_{(j-1)_+}} + \boldsymbol{\mu}^T \frac{\partial \boldsymbol{\chi}}{\partial t_{(j-1)_+}} \right) \delta t_{(j-1)_+} \\
& + \left(H_{j_-} + \frac{\partial \varphi}{\partial t_{j_-}} + \boldsymbol{\mu}^T \frac{\partial \boldsymbol{\chi}}{\partial t_{j_-}} \right) \delta t_{j_-} \\
& + \left(\boldsymbol{\lambda}^T_{(j-1)_+} + \frac{\partial \varphi}{\partial \mathbf{x}_{(j-1)_+}} + \boldsymbol{\mu}^T \left[\frac{\partial \boldsymbol{\chi}}{\partial \mathbf{x}_{(j-1)_+}} \right] \right) \delta \mathbf{x}_{(j-1)_+} \\
& + \left(-\boldsymbol{\lambda}^T_{j_-} + \frac{\partial \varphi}{\partial \mathbf{x}_{j_-}} + \boldsymbol{\mu}^T \left[\frac{\partial \boldsymbol{\chi}}{\partial \mathbf{x}_j} \right] \right) \delta \mathbf{x}_{j_-} \\
& + \int_{t_{(j-1)_+}}^{t_j} \left(\left(\frac{\partial H}{\partial \mathbf{x}} + \dot{\boldsymbol{\lambda}}^T \right) \delta \mathbf{x} + \frac{\partial H}{\partial \mathbf{u}} \delta \mathbf{u} \right) \mathrm{d}t \qquad j = 1, \dots, n,
\end{aligned}
\tag{4.5}
$$

where the Hamiltonian of the system has been introduced

$$H = \boldsymbol{\lambda}^T \mathbf{f}. \tag{4.6}$$

For each permissible variation along the path ($\delta \mathbf{x}$ and $\delta \mathbf{u}$), as well as at boundary points ($\delta \mathbf{x}_{(j-1)_+}$, $\delta \mathbf{x}_{j_+}$, $\delta t_{(j-1)_+}$, δt_{j_-}), the first variation of J^* must be null as a necessary condition for optimality.

The *Euler–Lagrange equations* for adjoint variables (Equation (4.7)) and algebraic equations for the control variables (Equation (4.8)) are obtained by nullifying the coefficients of $\delta \mathbf{x}$ and $\delta \mathbf{u}$:

$$\frac{\mathrm{d}\boldsymbol{\lambda}}{\mathrm{d}t} = -\left(\frac{\partial H}{\partial x} \right)^T \tag{4.7}$$

$$\left(\frac{\partial H}{\partial \mathbf{u}} \right)^T = 0 \tag{4.8}$$

Control variables are in general constrained, that is, they are limited to a specific admissible domain. The absolute value of thrust, for example, must be positive

and cannot exceed its maximum value T_{max}. In these cases, Equation (4.8) may not provide the optimal control. However, according to the *Pontryagin Maximum Principle*, the optimal control value in each point of the trajectory is the one that maximizes (if maxima for J are required) or minimizes (if minima for J are required) the Hamiltonian in that point and falls in the admissible domain. The system exhibits a peculiarity if the Hamiltonian is linear with respect to one of the constrained controls. Indeed, since the control does not appear explicitly in the Equation (4.8), it cannot be determined. In this circumstance, there are two alternatives:

- if, in Equation (4.6), the constrained control coefficient is not null, the Hamiltonian is maximized with the maximum value for the control when the coefficient is positive, or with the minimum one when the coefficient is negative. This is commonly termed as bang-bang control;

- if, in Equation (4.6), the constrained control coefficient is null, a (*singular arc*) occurs. The cancellation of every derivative of the coefficient itself, with respect to time, must then be imposed until one of them does not explicitly contain the control. After that, the optimal control is obtained by placing the last derivative to null.

Finally, the coefficients of $\delta\mathbf{x}_{(j-1)_+}, \delta\mathbf{x}_{j_-}, \delta t_{(j-1)_+}, \delta t_{j_-}$ are nullified to obtain the optimum boundary conditions:

$$-\boldsymbol{\lambda}_{j_-}^T + \frac{\partial\varphi}{\partial\mathbf{x}_{j_-}} + \boldsymbol{\mu}^T \left[\frac{\partial\boldsymbol{\chi}}{\partial\mathbf{x}_{j_-}}\right] = 0 \qquad j = 1,\ldots,n \ , \tag{4.9}$$

$$\boldsymbol{\lambda}_{j_+}^T + \frac{\partial\varphi}{\partial\mathbf{x}_{j_+}} + \boldsymbol{\mu}^T \left[\frac{\partial\boldsymbol{\chi}}{\partial\mathbf{x}_{j_+}}\right] = 0 \qquad j = 0,\ldots,n-1 \ , \tag{4.10}$$

$$H_{j_-} + \frac{\partial\varphi}{\partial t_{j_-}} + \boldsymbol{\mu}^T \frac{\partial\boldsymbol{\chi}}{\partial t_{j_-}} = 0 \qquad j = 1,\ldots,n \ , \tag{4.11}$$

$$-H_{j_+} + \frac{\partial\varphi}{\partial t_{j_+}} + \boldsymbol{\mu}^T \frac{\partial\boldsymbol{\chi}}{\partial t_{j_+}} = 0 \qquad j = 0,\ldots,n-1 \ . \tag{4.12}$$

By removing the constants Lagrange multipliers from the previous set of Equations (4.9 - 4.12), optimum boundary conditions and the ones imposed on the state variables, given by Equation (4.2), can be collected in a single vector $\boldsymbol{\sigma}$:

$$\boldsymbol{\sigma}\left(\mathbf{x}_{(j-1)_+}, \mathbf{x}_{j_-}, \boldsymbol{\lambda}_{(j-1)_+}, \boldsymbol{\lambda}_{j_-}, t_{(j-1)_+}, t_{j_-}\right) = 0 \qquad j = 1,\ldots,n \tag{4.13}$$

Equation (4.13), together with the state (4.1) and adjoint (4.7) differential equations describes a multipoint boundary value problem (MPBVP).

33

4.2   Boundary Value Problem

According to the optimal control theory, the optimization problem is formulated as a Boundary Value Problem (BVP) in which some of the variables' initial values are unknowns. The solution to this problem consists in determining which initial values allow the boundary conditions (imposed and optimal) to be satisfied, once the set of differential equations is integrated.

The described problem is characterized by some peculiarities:

- arches are used to split the integration domain into subintervals. The differential equations' formulation is constant within each arch, but it may differ from one arch to the next;

- in general, the duration of each arch is unspecified;

- boundary conditions can be non-linear and include the variables' value at both the external and internal boundaries;

- at the internal boundaries, the variables may be discontinuous, and their values after this discontinuity may be unknown.

The solution of Boundary Values Problems is the main challenge when dealing with indirect optimization methods. This solution is found by breaking down the BVP into a series of sub-problems, which are then solved using the well-known *Newton method*.

To overcome the problem of the arches' duration being indefinite, the independent variable t is substituted with a new variable ε, which, in the jth arc, is defined as:

$$\varepsilon = j - 1 + \frac{t - t_{j-1}}{t_j - t_{j-1}} = j - 1 + \frac{t - t_{j-1}}{\tau_j}$$

where τ_j is the unkown duration of the jth subinterval. Internal and external boundaries are therefore established.

The resolution method is described considering a general system of equations (given by Equations (4.1) and (4.7)), with controls replaced by expression (4.8):

$$\frac{\mathrm{d}\mathbf{y}}{\mathrm{d}t} = \mathbf{f}^*(\mathbf{y}, t) \tag{4.14}$$

where state and adjoint variables have been gathered in a new variable vector $\mathbf{y} = (\mathbf{x}, \boldsymbol{\lambda})$. Constant parameters, such as the duration of subintervals τ_j, are also present in the stated problem; consequently, it is convenient to consider a new vector $\mathbf{z} = (\mathbf{y}, \mathbf{c})$, which includes state variables, adjoint variables, and constant

parameters.

Thus, the differential equations system can be written as:

$$\frac{\mathrm{d}\mathbf{z}}{\mathrm{d}\varepsilon} = \mathbf{f}(\mathbf{z}, \varepsilon) \tag{4.15}$$

Considering the state and adjoint variables vector, the second member of Equation (4.15) can be expressed as:

$$\frac{\mathrm{d}\mathbf{y}}{\mathrm{d}\varepsilon} = \tau_j \frac{\mathrm{d}\mathbf{y}}{\mathrm{d}t} \tag{4.16}$$

while for the constants' vector, the second member of Equation (4.15) is clearly null:

$$\frac{\mathrm{d}\mathbf{c}}{\mathrm{d}\varepsilon} = 0 \tag{4.17}$$

The imposed and optimal boundary conditions are usually expressed as:

$$\Psi(\mathbf{s}) = 0 \tag{4.18}$$

where, the $\mathbf{y}$ vector's values at the external and internal boundaries and the constant parameters are included in the vector $\mathbf{s}$:

$$\mathbf{s} = (\mathbf{y_0}, \ldots, \mathbf{y_n}, \mathbf{c}) \tag{4.19}$$

Some of the state and adjoint variables' initial values are unknown, as well as several constant parameters. To determine the unknowns that allow the boundary conditions to be satisfied, an iterative procedure is used. The methodology is here described considering all of the initial values as unknown; obviously, it becomes simpler if one or more initial values are explicitly defined.

Initially, tentative values are assumed; it is critical that these starting values are sufficiently close to the optimal solution to ensure convergence. After the first iteration, the initial values are those obtained at the conclusion of the previous iteration. Thus, if the rth iteration is running, the following equality holds:

$$\mathbf{z}(0) = \mathbf{p}^r \tag{4.20}$$

where $\mathbf{p}^r$ are the rth iteration's initial values.

The numerical integration of equations (4.15) is the first step; values of the state variables are determined at each boundary, and the error on the boundary conditions $\mathbf{\Psi}^r$ is obtained. Thus, a variation $\Delta\mathbf{p}$ on the initial values is required: this variation causes changes to the error on the boundary conditions $\Delta\mathbf{\Psi}$, which can be written as:

$$\Delta\mathbf{\Psi} = \left[\frac{\partial\mathbf{\Psi}}{\partial\mathbf{p}}\right]\Delta\mathbf{p} \tag{4.21}$$

In order to satisfy Equation (4.18), it is necessary that $\Delta\boldsymbol{\Psi} = -\boldsymbol{\Psi}^r$. That is, the variation on the initial values can be expressed as:

$$\Delta\mathbf{p} = \mathbf{p}^{r+1} - \mathbf{p}^r = -\left[\frac{\partial\boldsymbol{\Psi}}{\partial\mathbf{p}}\right]^{-1}\boldsymbol{\Psi}^r \tag{4.22}$$

This process is followed until the boundary conditions are fulfilled with the required accuracy.

The matrix derived in the second term of equation (4.22) can be obtained both analytically and numerically.

If the analytical approach is considered, it is useful to write the matrix as the product of two matrices

$$\left[\frac{\partial\boldsymbol{\Psi}}{\partial\mathbf{p}}\right] = \left[\frac{\partial\boldsymbol{\Psi}}{\partial\mathbf{s}}\right]\left[\frac{\partial\mathbf{s}}{\partial\mathbf{p}}\right] \tag{4.23}$$

where the first may be easily calculated by deriving the boundary conditions with regard to the involved variables. The second matrix, on the other hand, comprises the boundary values of:

$$\left[\frac{\partial\mathbf{z}}{\partial\mathbf{p}}\right] = [\mathbf{g}(\varepsilon)] \tag{4.24}$$

This is derived by integrating the system of differential equations (4.15) with respect to the initial values:

$$[\dot{g}] = \frac{\mathrm{d}}{\mathrm{d}\varepsilon}\left[\frac{\partial\mathbf{z}}{\partial\mathbf{p}}\right] = \left[\frac{\partial}{\partial\mathbf{p}}\left(\frac{\mathrm{d}\mathbf{z}}{\mathrm{d}\varepsilon}\right)\right] = \left[\frac{\partial\mathbf{f}}{\partial\mathbf{p}}\right] \tag{4.25}$$

Equation (4.25) can be reformulated by exploiting the principal system's *Jacobian*:

$$[\dot{\mathbf{g}}] = \left[\frac{\partial\mathbf{f}}{\partial\mathbf{z}}\right]\left[\frac{\partial\mathbf{z}}{\partial\mathbf{p}}\right] = \left[\frac{\partial\mathbf{f}}{\partial\mathbf{z}}\right][\mathbf{g}] \tag{4.26}$$

As mentioned, the matrix derived in the second term of equation (4.22) can also be obtained numerically. In fact, adding a certain Δp to the ith component of $\mathbf{p}$ and proceeding with the integration of Equation (4.15), it is possible to derive the related change in the boundary conditions $\Delta\boldsymbol{\Psi}(\Delta p)$. Thus, through linearization, it is possible to calculate the corresponding row as: $\Delta\boldsymbol{\Psi}^T/\Delta p$. In general, the numerical procedure allow to reduce the computational time. However, the convergence of this method is not certain.

The linearization used to determine the correction $\Delta\mathbf{p}$, given by Equation (4.22), introduces inaccuracies that may invalidate the method's convergence. Steps to improve the procedure have been implemented to avoid this issue:

- The applied correction $\Delta\mathbf{p}$ is just a fraction of the one calculated by equation (4.22):

$$\mathbf{p}^{r+1} = \mathbf{p}^r + K_1\Delta\mathbf{p} \tag{4.27}$$

  where $K_1 \in [0.1, 1]$.
  This can prevent the adopted procedure from moving away from the solution of the problem.

- At each iteration, the maximum error on the boundary conditions E_{max}^{r+1} is compared to the one calculated in previous iteration E_{max}^r. If

$$E_{max}^{r+1} < K_2 E_{max}^r$$

  the next iteration can be performed. Since the boundary conditions' error may grow in the first iterations, the value of K_2 must be greater than one. In general $K_2 \in [2, 3]$.

- If the error on the boundary conditions, associated with the most recent iteration, is too high in comparison to the prior one, the correction is bisectioned. That is:

$$\mathbf{p}^{r+1} = \mathbf{p}^r + K_1\Delta\mathbf{p}/2 \tag{4.28}$$

  The new error is then compared to the previous one. If necessary, the bisection may be applied again, with a maximum of 5 times. If the new error remains greater than the old one, then the calculation is stopped.

Chapter 5

Problem Statement

Notions and generic equations described in the previous chapter are applied to the missions covered in this study. Moreover, reference parameters to formulate the problem in a dimensionless form are provided. Finally, a set of suitable boundary conditions is given in order to define the mission.

The theoretical concepts presented in the following chapter are mainly based on the works of professors Casalino [20] and Colasurdo [5], and professor Prussing [21].

5.1   Space Trajectories Optimization

A heliocentric reference system is adopted to study optimal trajectories, and, given the considerations highlighted in Chapter 3, the problem may be analysed using the approximation of the Two-Body Problem. Indeed, the hypothesis of a point mass spacecraft under the effect of a single body is commonly used in preliminary study of spacecraft trajectories. Moreover, since the patched-conic approximation is frequently utilized in the early studies, the two-body model can be used to deal with the investigated interplanetary trajectories. Only the heliocentric legs are considered; at the patch points with the planetocentric legs, proper boundary conditions take into account the manoeuvres within the planets' spheres of influence. The state of the spacecraft is described by position $\mathbf{r}$, velocity $\mathbf{v}$, and mass m, and the state equations are:

$$\frac{d\mathbf{r}}{dt} = \mathbf{v}, \tag{5.1}$$

$$\frac{d\mathbf{v}}{dt} = \mathbf{g} + \frac{\mathbf{T}}{m}, \tag{5.2}$$

$$\frac{dm}{dt} = -\frac{T}{c}, \tag{5.3}$$

where $\mathbf{r}$ is the position vector of the satellite with respect to the Sun, $\mathbf{v}$ is the velocity vector of the spacecraft and $\mathbf{T}$ is the thrust vector. $\mathbf{g}$ is the gravitational acceleration, that can be expressed as $\mathbf{g} = -\mu_{\odot}\mathbf{r}/r^3$, where $\mu_{\odot}$ is the Sun's gravitational parameter. The propellant mass-flow rate is expressed by the ratio of the thrust magnitude to the constant effective exhaust velocity c.

As mentioned, according to the *Theory of Optimal Control*, the Hamiltonian can be stated as:

$$H = \boldsymbol{\lambda}^T \mathbf{f}, \tag{5.4}$$

and substituting the state equations, the following expression is obtained

$$H = \boldsymbol{\lambda}_{\mathbf{r}}^T \mathbf{v} + \boldsymbol{\lambda}_{\mathbf{v}}^T \left(\mathbf{g} + \frac{T}{m}\mathbf{u} \right) - \lambda_m \frac{T}{c}, \tag{5.5}$$

where $\mathbf{u}$, a unit vector in the thrust direction, has been introduced.

The thrust direction and magnitude are typically the control variables, and according to the *Pontryagin Maximum Principle*, H must be maximized in order to maximize the performance index J.

By inspection, the Hamiltonian is thus maximized over the choice of thrust direction by aligning the unit vector $\mathbf{u}$ parallel to the adjoint vector $\boldsymbol{\lambda}_{\mathbf{v}}$. Because of the significance of the vector $\boldsymbol{\lambda}_{\mathbf{v}}$, Lawden [3] termed it the *primer vector* $\boldsymbol{\lambda}_{\mathbf{V}}$.

The optimal thrust unit vector is then in the direction of the primer vector, specifically:

$$\mathbf{u} = \frac{\boldsymbol{\lambda}_{\mathbf{V}}}{\lambda_V} \tag{5.6}$$

Moreover, introducing the *Switching Function*:

$$S_F = \frac{\boldsymbol{\lambda}_{\mathbf{v}}^T}{m}\mathbf{u} - \frac{\lambda_m}{c} = \frac{\lambda_V}{m} - \frac{\lambda_m}{c}, \tag{5.7}$$

equation (5.5) can be rewritten as:

$$H = \boldsymbol{\lambda}_{\mathbf{r}}^T \mathbf{v} + \boldsymbol{\lambda}_{\mathbf{v}}^T \mathbf{g} + T S_f \tag{5.8}$$

Thus, to maximize the Hamiltonian over the choice of the thrust magnitude T, the following control law is assumed:

$$T = \begin{cases} T_{max} & \text{for} \quad S_F > 0 \\ 0 & \text{for} \quad S_F < 0 \end{cases}, \tag{5.9}$$

that is, the thrust magnitude switches between its limiting values of 0 (an NT *null thrust* arc) and T_{max} (an MT *maximum-thrust arc*) each time $S_F(t)$ passes through 0 according to Equation (5.9) [21]. Figure 5.1 shows an example switching function for a three-burn trajectory.
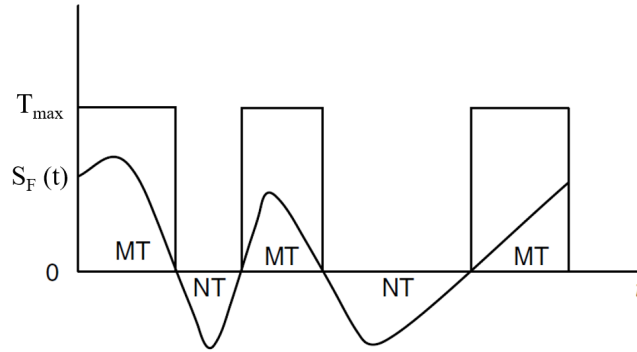
Figure 5.1: Three-burn switching function and thrust profile [21]

When S_F remains 0 for a finite period of time, singular arcs arise. In this cases, equation (5.8) is not sufficient to decide the optimal thrust magnitude. However, singular arcs are here excluded because, generally, they may be required during atmospheric flight.

5.2 Equations in spherical coordinates

Vectorial equations must be projected onto a suitable reference system of coordinate. Considering the absence of Coriolis and inertial accelerations, choosing an inertial reference frame is the best option. A spherical set of coordinates is adopted within this reference frame (Figure 5.2). The equatorial plane of the central body — in this case, the Sun — serves as the basis for this reference frame.
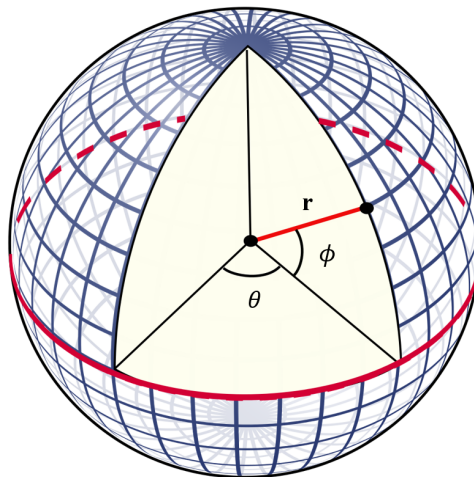
Figure 5.2: Spherical coordinates [22]

The *position vector* of the spacecraft, within this coordinate system, can be expressed as:

$$\mathbf{r} = \begin{bmatrix} r \\ \theta \\ \phi \end{bmatrix} \tag{5.10}$$

where r is the distance from the Sun, θ is the longitude and ϕ is the latitude. The *velocity vector* is written using local *East, North, Up (ENU)* coordinates :

$$\mathbf{v} = \begin{bmatrix} u \\ v \\ w \end{bmatrix}. \tag{5.11}$$

Figure 5.3 shows the physical orientation of the velocity components,
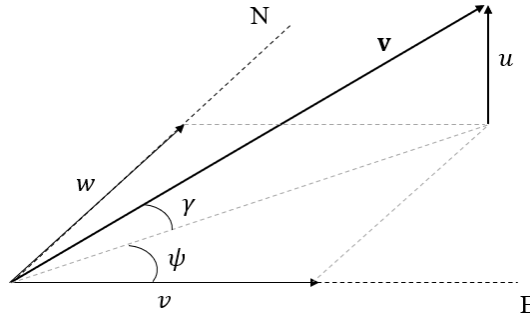
Figure 5.3: Velocity components in the horizon (N-E) plane

where γ and ψ represent the *flight path angle* and the *heading angle* respectively. As a result, the state vector may be expressed as:

$$\mathbf{x} = \begin{bmatrix} r \\ \theta \\ \phi \\ u \\ v \\ w \\ m \end{bmatrix}. \tag{5.12}$$

Projecting the state equations in the chosen reference frame, the following expressions are obtained:

$$\frac{\mathrm{d}r}{\mathrm{d}t} = u \tag{5.13}$$

$$\frac{\mathrm{d}\theta}{\mathrm{d}t} = \frac{v}{r\cos\phi} \tag{5.14}$$

$$\frac{\mathrm{d}\phi}{\mathrm{d}t} = \frac{w}{r} \tag{5.15}$$

$$\frac{\mathrm{d}u}{\mathrm{d}t} = -\frac{1}{r^2} + \frac{v^2}{r} + \frac{w^2}{r} + \frac{T}{m}\sin\gamma_T \tag{5.16}$$

$$\frac{\mathrm{d}v}{\mathrm{d}t} = -\frac{uv}{r} + \frac{wv}{r}\tan\phi + \frac{T}{m}\cos\gamma_T\cos\psi_T \tag{5.17}$$

$$\frac{\mathrm{d}v}{\mathrm{d}t} = -\frac{uv}{r} + \frac{wv}{r}\tan\phi + \frac{T}{m}\cos\gamma_T\cos\psi_T \tag{5.18}$$

$$\frac{\mathrm{d}w}{\mathrm{d}t} = -\frac{uw}{r} - \frac{v^2}{r}\tan\phi + \frac{T}{m}\cos\gamma_T\sin\psi_T \tag{5.19}$$

$$\frac{\mathrm{d}m}{\mathrm{d}t} = -\frac{T}{c} \tag{5.20}$$

where γ_T and ψ_T are respectively the thrust *flight path angle* and *heading angle*, which represent the controls that determine the thrust's direction.

The Hamiltonian's expression can also be reformulated:

$$
\begin{aligned}
H = {}& \lambda_r u + \lambda_\theta \frac{v}{r\cos\phi} + \lambda_\phi \frac{w}{T} + \\
& + \lambda_u \left(-\frac{\mu}{r^2} + \frac{v^2}{T} + \frac{w^2}{T} + \frac{T}{m}\sin\gamma_T \right) + \\
& + \lambda_v \left(-\frac{uv}{r} + \frac{vw}{r}\tan\phi + \frac{T}{m}\cos\gamma_T\cos\psi_T \right) + \\
& + \lambda_w \left(-\frac{uw}{r} - \frac{v^2}{r}\tan\phi + \frac{T}{m}\cos\gamma_T\sin\psi_T \right) - \lambda_m \frac{T}{c}
\end{aligned}
\tag{5.21}
$$

It is thus possible to derive the optimal values of γ_T and ψ_T by imposing equal to null the partial derivatives of the Hamiltonian, based on what was discussed in the previous chapter. Mathematically:

$$\left(\frac{\partial H}{\partial \mathbf{u}} \right)^T = 0 \tag{5.22}$$

where $\mathbf{u} = [\gamma_T \ \psi_T]$ is the *control vector*.

Equations (5.23, 5.24, 5.25) formulate optimal values for the control variables.

$$\sin \gamma_T = \frac{\lambda_u}{\lambda_V} \tag{5.23}$$

$$\cos \gamma_T \cos \psi_T = \frac{\lambda_v}{\lambda_V} \tag{5.24}$$

$$\cos \gamma_T \sin \psi_T = \frac{\lambda_w}{\lambda_V} \tag{5.25}$$

where

$$\lambda_V = \sqrt{\lambda_u^2 + \lambda_v^2 + \lambda_w^2} \tag{5.26}$$

is the primer vector's absolute value.

The differential equations for adjoint variables $\boldsymbol{\lambda} = [\lambda_r \; \lambda_\theta \; \lambda_\phi \; \lambda_u \; \lambda_v \; \lambda_w \; \lambda_m]$ are the last remaining set of equations to be defined. These are provided by the *Euler-Lagrange* equations:

$$\frac{\mathrm{d}\boldsymbol{\lambda}}{\mathrm{d}t} = -\left(\frac{\partial H}{\partial \boldsymbol{x}}\right)^T \tag{5.27}$$

which, for the analysed problem, gives:

$$\dot{\lambda}_r = \frac{1}{r^2}\left[\lambda_\theta \frac{v}{\cos\phi} + \lambda_\phi w + \lambda_u \left(-\frac{2}{r} + v^2 + w^2\right) + \right.$$
$$\left. + \lambda_v(-uv + vw\tan\phi) + \lambda_w\left(-uw - v^2\tan\phi\right)\right] \tag{5.28}$$

$$\dot{\lambda}_\theta = 0 \tag{5.29}$$

$$\dot{\lambda}_\phi = \frac{1}{r\cos^2\phi}\left(-\lambda_\theta v\sin\phi - \lambda_v vw + \lambda_w v^2\right) \tag{5.30}$$

$$\dot{\lambda}_u = \frac{1}{r}\left(-\lambda_r r + \lambda_v v + \lambda_w w\right) \tag{5.31}$$

$$\dot{\lambda}_v = \frac{1}{r}\left[-\lambda_\theta \frac{1}{\cos\phi} - 2\lambda_u v + \lambda_v(u - w\tan\phi) + 2\lambda_w v\tan\phi\right] \tag{5.32}$$

$$\dot{\lambda}_w = \frac{1}{r}\left(-\lambda_\phi - 2\lambda_u w - \lambda_v v\tan\phi + \lambda_w u\right) \tag{5.33}$$

$$\dot{\lambda}_m = \frac{T}{m^2}\lambda_V \tag{5.34}$$

43

5.3   Dimensionless quantities

Reference quantities to formulate the problem in a dimensionless form are presented in this section. Reference values for distance, time, velocity, acceleration, and mass are provided. As a consequence, every dimensionless quantity presented in this work may be expressed in dimensional form, by exploiting these reference values.

5.3.1   Distance reference value

The astronomical unit

$$1 \text{ AU} = 149597870.7 \text{ km} \quad,$$

defined as the mean distance between the Earth and the Sun, serves as a distance reference. This allows to work with numbers in the order of units, instead of several millions of kilometers. As a matter of fact, analysing trips to NEAs, the spacecraft's distance from the Sun seldom surpasses 3 AU or goes below 0.7 AU. Therefore, the reference distance is exactly:

$$r_{conv} = 1 \text{ AU}$$

5.3.2   Time reference value

One (*sidereal*) year represent a complete revolution of the Earth around the Sun; in other word, Earth covers a 2π rad angle in one sidereal year:

$$1 \text{ year} \rightarrow 2\pi \text{ rad}$$

Radians can therefore be used to measure time instead of years.
As a result of this consideration, the reference time can thus be defined as:

$$t_{conv} = \frac{365 \text{ days}}{2\pi} = 58.13244088 \text{ days}$$

Epoch *J*2000, a standard point in time used as a reference in astronomy, is employed as the starting date from which time is measured. *J*2000 is precisely defined as an exact point that is very close to noon, January 1, 2000 GMT, i.e., precisely Julian date 2451545.0. Thus, for example,

$$\text{if dimensionless } t = 138.9927 \longrightarrow \text{ date} = 14/2/2022$$

5.3.3   Velocity reference value

Based on what has been discussed about distances taking on a dimensionless form, it is straightforward to assume that velocities will be linked to a characteristic

velocity of the Earth's orbit. In practice, all velocities are expressed as a multiple of the Earth's circular velocity, which is defines as:

$$V_{conv} = \sqrt{\frac{\mu_\odot}{r_{conv}}} = 29.784642455 \text{ km/s}$$

With this option, all of the velocities are around 1, hence the reason for this decision is similar to that of the dimensionless distance.

5.3.4   Acceleration and mass reference values

The reference acceleration can once again be found by looking at the Earth's orbit. Indeed, it is expressed as:

$$a_{conv} = \frac{\mu_\odot}{r_{conv}^2} = 5.930063858 \times 10^{-6} \text{ km/s}^2$$

In terms of mass, the starting mass of the spacecraft serves as a reference point. Thus, the mass will be equal to 1 at the start of the mission, and the end mass will be equal to the ratio of the final and starting masses.

5.4   Boundary Conditions

Once the set of differential equations and the dimensionless parameters have been determined, it is required to introduce the problem's boundary conditions. As previously stated, the proposed space mission departs from Earth at time t_0 and visits N asteroids at different dates t_N, with at most, $N = 3$. A rendezvous manoeuvre is executed for each asteroid, with a stay duration of about two months; after that, the spacecraft will continue its journey towards the next asteroid. Thus, diverse boundary conditions can be specified at main points during the mission. In particular, considering the more generic type of mission ($N = 3$), the following points will be constrained:

- Departure from Earth → **0**

- Arrival to the first asteroid → **1**−

- Departure from the first asteroid → **1**+

- Arrival to the second asteroid → **2**−

- Departure from the second asteroid → **2**+

- Arrival to the third, and final, asteroid → **f**

Departure From Earth

The following constraints for the spacecraft's position and velocity vectors and for its initial mass may be applied at the time of departure from Earth:

$$\mathbf{r}(t_0) = \mathbf{r}_{\text{Earth}}(t_0)$$

$$\mathbf{v}(t_0) = \mathbf{v}_{\text{Earth}}(t_0)$$

In other words, spacecraft position and velocity are assumed identical to those of the Earth at time t_0, even though its journey begins outside the Earth's sphere of influence. This is possible since the sphere of influence's dimension is relatively small compared to the distance between Earth and Sun, thus can be neglected. Clearly, at the beginning of the mission the initial mass is:

$$m(t_0) = 1$$

More properly, the initial mass is typically a function of the hyperbolic excess velocity $\mathbf{v}_{\infty_0} = \mathbf{v}(t_0) - \mathbf{v}_{\text{Earth}}(t_0)$ [5]:

$$m(t_0) = f(\mathbf{v}_{\infty_0})$$

Arrival at/Departure from the first asteroid

Keeping in mind the previous argument, the spacecraft's position and velocity at the conclusion of the first arc must be the same as the first asteroid:

$$\mathbf{r}(t_{1-}) = \mathbf{r}_{\text{asteroid}_1}(t_{1-})$$

$$\mathbf{v}(t_{1-}) = \mathbf{v}_{\text{asteroid}_1}(t_{1-})$$

The second arc begins at t_{1+}, after a stay of around two months. Thus t_{1+} is defined as:

$$t_{1+} = t_{1-} + t_{stay_1}$$

The following boundary conditions apply while departing from the first asteroid:

$$\mathbf{r}(t_{1+}) = \mathbf{r}_{\text{asteroid}_1}(t_{1+})$$

$$\mathbf{v}(t_{1+}) = \mathbf{v}_{\text{asteroid}_1}(t_{1+})$$

Considering no propellant consumption throughout the stay duration, between t_{1-} and t_{1+} the spacecraft's mass remains constant:

$$m(t_{1+}) = m(t_{1-})$$

Arrival at/Departure from the second asteroid

The second arc comes to an end when the second asteroid is reached (t_{2-}). The spacecraft's position and velocity vectors must be the same as the second asteroid at this time:

$$\mathbf{r}(t_{2-}) = \mathbf{r}_{\text{asteroid}_2}(t_{2-})$$

$$\mathbf{v}(t_{2-}) = \mathbf{v}_{\text{asteroid}_2}(t_{2-})$$

The third arc begins at t_{2+}, after a stay of around two months. Thus t_{2+} is defined as:

$$t_{2+} = t_{2-} + t_{stay_2}$$

While leaving the second asteroid, the following boundary conditions apply:

$$\mathbf{r}(t_{2+}) = \mathbf{r}_{\text{asteroid}_2}(t_{2+})$$

$$\mathbf{v}(t_{2+}) = \mathbf{v}_{\text{asteroid}_2}(t_{2+})$$

Again, no propellant consumption is taken into account for the duration of the stay, therefore:

$$m(t_{2+}) = m(t_{2-})$$

Arrival to the final asteroid

The final asteroid's arrival is clearly handled the same as the previous ones; the spacecraft must present the final target's position and velocity vectors. Mathematically:

$$\mathbf{r}(t_f) = \mathbf{r}_{\text{asteroid}_f}(t_f)$$

$$\mathbf{v}(t_f) = \mathbf{v}_{\text{asteroid}_f}(t_f)$$

The final mass m_f is the performance index which is maximized.

Chapter 6

Resolution methods

As previously stated, the problem presented in this thesis is solved via an indirect optimization algorithm that makes use of shooting techniques. The numerical code's Flowchart is depicted in Figure 6.1.

The code's executable file requires a set of data inputs to begin the analysis. In particular:

- calculation's parameters, as: number of iterations, K_1 and K_2 parameters introduced in Chapter 4;

- spacecraft's features, as: thrust coefficient, initial mass;

- trajectory's characteristics, as: mission duration, departure time from Earth, arrival time to intermediate asteroid(s), stay duration.

A text file providing the solution's initial guess is also needed. The convergence to the optimum is typically obtained if the tentative solution is sufficiently close to the optimal one.

In this chapter, suitable procedures to define the initial guess and then to find multiple optimized rendezvous missions are described.

First, the tentative solution's general structure is presented. The methodology for identifying target asteroids is next discussed. In the following section, procedures for estimating the initial guess to quickly obtain solutions are detailed. Since the current work searches missions to one, two, or three targets, the estimation of tentative solutions must be carried out separately for each of these scenarios. Finally, the obtained solutions are corrected by analysing the switching function profile.

6.1 Tentative Solution Definition

Initial conditions are contained in the tentative solution file, whose general form for the analysed case is:

$$
\begin{bmatrix}
t_0 & t_1 & \lambda_{\theta_{0-1}} \\
t_2 & \lambda_{\theta_{1-2}} & t_3 \\
\lambda_{\theta_{2-3}} & t_4 & \lambda_{\theta_{3-4}} \\
t^* & & \\
t_{stay_i} & & \\
r_i & \theta_i & \phi_i \\
u_i & v_i & w_i \\
\lambda_{ri} & \lambda_{\phi i} & \lambda_{ui} \\
\lambda_{vi} & \lambda_{wi} & V_{\infty 0} \\
r_0 & \theta_0 & \phi_0 \\
u_0 & v_0 & w_0 \\
\lambda_{r0} & \lambda_{\phi 0} & \lambda_{u0} \\
\lambda_{v0} & \lambda_{w0} & m_0
\end{bmatrix}
\qquad \text{with } i = 1, 2, 3
$$

where:

- $[t_0\ t_1,\ t_2,\ t_3,\ t_4,\ t^*]$ are respectively the departure time, the first, second, and third rendezvous timings, the arrival time, and the *optimal* time to perform the mission;

- $[\lambda_{\theta_{0-1}},\ \lambda_{\theta_{1-2}},\ \lambda_{\theta_{2-3}}, \lambda_{\theta_{3-4}}]$ are respectively the value of λ_θ for the first, second, third and fourth arc. Indeed, in each arc the adjoint variable λ_θ is constant.

- $[t_{stay_1},\ t_{stay_2},\ t_{stay_3}]$ are the stay time at each *intermediate* asteroid. The t_{stay_i} is defined as the departure time from the ith *intermediate* asteroid minus the arrival time at the ith *intermediate* asteroid.

- $[r_0, \theta_0, \phi_0, u_0, v_0, w_0, \lambda_{r_0}, \lambda_{\phi_0}, \lambda_{u_0}, \lambda_{v_0}, \lambda_{w_0}]$ are the state and adjoint variables at the departure.

- $[r_1, \theta_1, \phi_1, u_1, v_1, w_1, \lambda_{r_1}, \lambda_{\phi_1}, \lambda_{u1}, \lambda_{v1}, \lambda_{w1}]$ are the state and adjoint variables at the departure from the first *intermediate* asteroid.

- $[r_2, \theta_2, \phi_2, u_2, v_2, w_2, \lambda_{r_2}, \lambda_{\phi_2}, \lambda_{u2}, \lambda_{v2}, \lambda_{w2}]$ are the state and adjoint variables at the departure from the second *intermediate* asteroid.

- $[r_3, \theta_3, \phi_3, u_3, v_3, w_3, \lambda_{r_3}, \lambda_{\phi3}, \lambda_{u3}, \lambda_{v3}, \lambda_{w3}]$ are the state and adjoint variables at the departure from the third *intermediate* asteroid.

- $[V_{\infty 0}, m_0]$ are the departure hyperbolic excess velocity and the initial mass.

49

This file represents the starting point for the integration of the differential equations. To obtain the desired solution, the initial guess has to be carefully constructed. The numerical method employed is indeed sensible to the variation of the initial conditions. At each iteration, the implemented numerical code updates the starting values according to the distance of the obtained solution from the boundary conditions imposed. Once the requested accuracy is obtained (boundary conditions error $\leq 10^{-7}$), the iterations stop and the optimal solution is found. If the initial guess is not precise enough, the numerical method does not converge and the error constantly grows: thus the iteration chain is stopped.
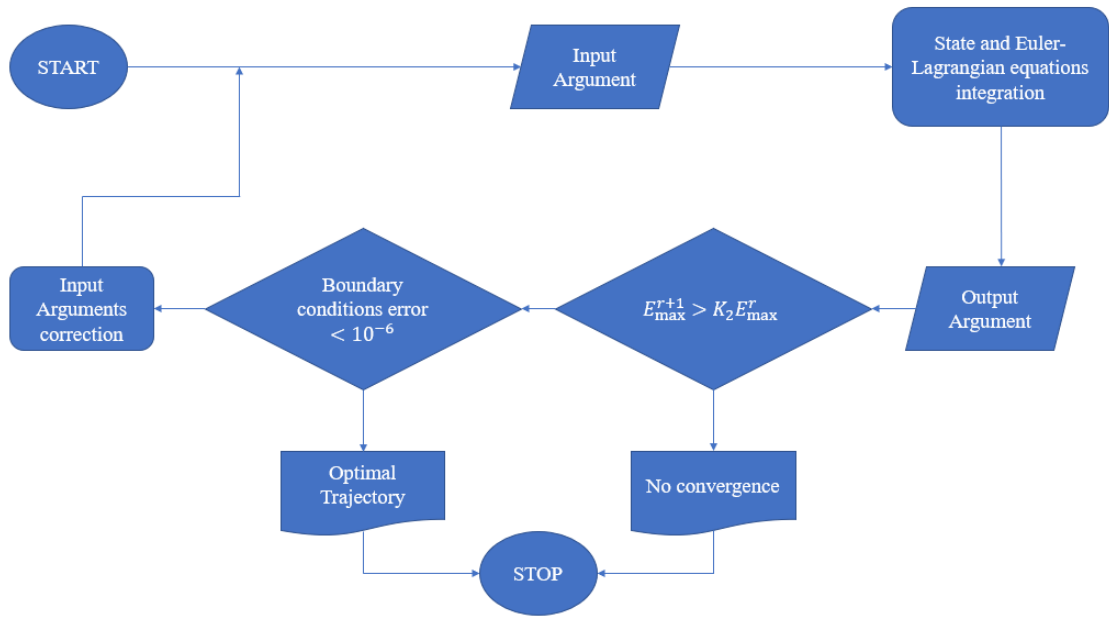
Figure 6.1: Numerical Code Flowchart

6.2 Target asteroids selection

A crucial step to perform the mission is the selection of the target asteroids. Based on what has been covered in Section 2.1.1, the number of potential targets is huge. For this reason, it is convenient to narrow the field to asteroids with suitable characteristics for the considered mission. To obtain solutions with a low propellant consumption and a reduced duration, asteroid's orbital parameters and their phase shift angles ($\Delta\theta$) with Earth are taken into account. This search is performed by exploiting the JPL Small-Body Elements Tables [23], which give:

- asteroid's name or designation, depending on whether the asteroid is Numbered

or Unnumbered;

- epoch of the elements represented as the Modified Julian Date (MJD), which is defined as the Julian date - 2400000.5

- semi-major axis of the orbit [AU];

- eccentricity of the orbit;

- inclination of the orbit with respect to the *J2000* ecliptic plane [deg];

- argument of perihelion (*J2000* - ecliptic) [deg];

- longitude of the ascending node (*J2000* - Ecliptic) [deg];

- mean anomaly at epoch [deg].

First of all, the selection based on the asteroid's orbital parameters is conducted, choosing asteroids with the following features:

1. semi-major axis:
$$0.80 AU < a < 1.20 AU;$$

2. eccentricity:
$$e < 0.20;$$

3. inclination:
$$i < 5°.$$

In the second place, a departure window from 2025 to 2035 has been fixed. Considering mission duration between two and four years, an arrival window to the target is also established. Thus, the analysis on the phase angles between Earth and selected asteroids, at arrival time, can be conducted. Starting with the mean anomaly at epoch (M_0) for each asteroid, the position after a time t can be calculated via

$$M = M_0 + \sqrt{\frac{\mu_\odot}{a^3}}\, t \qquad (6.1)$$

with $\mu_\odot$ being the gravitational constant of the Sun, and a being the semi-major axis of the asteroid. As mentioned in Chapter 3, to model the movement of celestial bodies on their orbit, Kepler's equation (3.14) is needed. There exists a number of ways to solve this equation, e.g. iterative methods like Newton's method and Halley's method. In this work the former is implemented. The root of the function:

$$f(E) = E - e \sin E - M = 0$$

has to be found. This leads to the iteration:

$$E_{i+1} = E_i - \frac{E_i - e \sin E_i - M}{1 - \cos E_i}$$

Once the eccentric anomaly E is found, the calculation of the *position vector*

$$\mathbf{r} = \begin{bmatrix} r \\ \theta \\ \phi \end{bmatrix}$$

of the asteroid, at specific arrival time, is straightforward. The same procedure is applied also for Earth; this allows the derivation of the phase shift angle ($\Delta\theta$) between Earth and asteroids.
Asteroids with a $\Delta\theta < 50°$ are chosen.

6.3 Tentative Solution estimation

Due to the intrinsic difficulty of trajectory optimization, convergence problems are generally not simple to manage. In these cases, the user's experience guides the convergence process, as each problem may require its peculiar approach [24].
In this section, procedures to estimate the initial guess to quickly obtain solutions are described. The present work searches missions to one, two or three targets; tentative solutions estimation has to be characterized for each of these cases separately.
For one-target missions, it can be easily found as further explained later on in this chapter. Initial guesses for two-target mission can be derived by exploiting one-target missions' tentative solution. Indeed, starting from the latter and "adding" an *intermediate* asteroid, the convergence is more easily achieved. Similarly, three-target missions' tentative solutions can be obtained from those used for two-target missions.

One-target missions

Since one-target missions have a lower number of unknown values, tentative solution structure is simplified. In particular:

$$\begin{bmatrix} t_0 & t_f & \lambda_{\theta_{0-1}} \\ t^* & & \\ V_{\infty 0} & r_0 & \theta_0 \\ \phi_0 & u_0 & v_0 \\ w_0 & \lambda_{r_0} & \lambda_{\phi_0} \\ \lambda_{u_0} & \lambda_{v_0} & \lambda_{w_0} \\ m_0 & & \end{bmatrix}$$

Given the considerations in Section 5.4, it is possible to define the position vector of the spacecraft at the departure

$$\mathbf{r_0} = \begin{bmatrix} r_0 \\ \theta_0 \\ \phi_0 \end{bmatrix}$$

once the initial time (t_0) is fixed. This is defined with respect to the arrival time (t_f) to the target and duration of the entire mission. V_{∞_0} is set null considering the spacecraft outside the Earth's sphere of influence at the departure time. The initial mass, expressed dimensionless, is $m_0 = 1$; t^* is fixed null, considering rendezvous missions. Concerning the adjoint variables, these are imposed to be small, but are not precisely defined.

Two-target missions

As previously stated, initial guesses for two-target missions can be generated from the solutions of one-target missions. The first step is to determine an intermediate asteroid to include in the spacecraft's journey, as well as an appropriate rendezvous time with it (t_1).

The appropriate intermediary asteroid must be chosen depending on the spacecraft's trajectory from Earth to the final destination. The implemented numerical code determines the temporal evolution of the spacecraft's position vector:

$$\mathbf{r(t)} = \begin{bmatrix} r(t) \\ \theta(t) \\ \phi(t) \end{bmatrix}$$

It is thus possible to calculate the relative position of asteroids in relation to the spacecraft using this data.

The selection of the intermediate asteroid is then made based on two primary criteria:

- its orbital parameters must be similar to those of the final target;

- at approximately half of the mission's duration, its relative position to the spacecraft must satisfy the following requirements:

$$\Delta r \leq k_1$$

$$\Delta \theta \leq k_2$$

$$\Delta \phi \leq k_3$$

with $k_1 = 0.1$ AU , $k2 = 15°$ and $k3 = 5°$.

Once the intermediate asteroid, as well as an appropriate rendezvous time with it, are obtained, the two-target mission's tentative solution can be derived. Its framework is:

$$
\begin{bmatrix}
t_0 & t_1 & \lambda_{\theta_{0-1}} \\
t_f & \lambda_{\theta_{1-2}} & \\
t^* & & \\
t_{stay1} & r_1 & \theta_1 \\
\phi_1 & u_1 & v_1 \\
w_1 & \lambda_{r1} & \lambda_{\phi_1} \\
\lambda_{u_1} & \lambda_{v_1} & \lambda_{w_1} \\
V_{\infty 0} & r_0 & \theta_0 \\
\phi_0 & u_0 & v_0 \\
w_0 & \lambda_{r_0} & \lambda_{\phi_0} \\
\lambda_{u_0} & \lambda_{v_0} & \lambda_{w_0} \\
m_0 & &
\end{bmatrix}
$$

In the first place, the one-target missions' initial guess must be edited replacing t_f with t_1.

One iteration of the implemented numerical code gives the unknown variables (r, θ, ϕ, u, v, w, λ_r, λ_ϕ, λ_u, λ_v, λ_w), at t_1. $\lambda_{\theta_{1-2}}$ can be set equal to $\lambda_{\theta_{0-1}}$ at first. t_{stay1} is set to null in order to force the old path to be followed. When this parameter is requested as an input from the numerical code executable file, however, it is set to one, implying that the stay time is nearly two months. All other unknown parameters are derived from the tentative solution of the single-target mission.

Three-target missions

Tentative solutions for three-target missions can be likewise derived from those regarding two-target missions. Starting with the spacecraft path for a two-target mission, the selection of a second intermediate asteroid can be carried out as previously explained.

Once the second intermediate asteroid, as well as an appropriate rendezvous time with it (t_2), are obtained, the three-target mission's tentative solution can be derived. Its framework is:

$$
\begin{bmatrix}
t_0 & t_1 & \lambda_{\theta_{0-1}} \\
t_2 & \lambda_{\theta_{1-2}} & t_f \\
\lambda_{\theta_{2-3}} \\
t^* \\
t_{stay1} & t_{stay2} & r_1 \\
\theta_1 & \phi_1 & u_1 \\
v_1 & w_1 & \lambda_{r1} \\
\lambda_{\phi_1} & \lambda_{u_1} & \lambda_{v_1} \\
\lambda_{w_1} & r_2 & \theta_2 \\
\phi_2 & u_2 & v_2 \\
w_2 & \lambda_{r2} & \lambda_{\phi_2} \\
\lambda_{u_2} & \lambda_{v_2} & \lambda_{w_2} \\
V_{\infty 0} & r_0 & \theta_0 \\
\phi_0 & u_0 & v_0 \\
w_0 & \lambda_{r_0} & \lambda_{\phi_0} \\
\lambda_{u_0} & \lambda_{v_0} & \lambda_{w_0} \\
m_0
\end{bmatrix}
$$

First, the two-target missions' initial guess must be edited replacing t_f with t_2. One iteration of the implemented numerical code gives the unknown variables (r, θ, ϕ, u, v, w, λ_r, λ_ϕ, λ_u, λ_v, λ_w), at t_2. $\lambda_{\theta_{2-3}}$ can be set equal to $\lambda_{\theta_{1-2}}$ at first. The definition of t_{stay2} is similar to that of t_{stay1}. It is initially set to null in order to force the old path to be followed; it is set to one when this parameter is requested as an input from the numerical code executable file. All other unknown parameters are derived from the tentative solution of the two-target mission.

6.4 Trajectory analysis based on switching function

Once convergence is achieved, the resulting solution may exhibit one or both of these shortcomings:

- $S_F(t_0) < 0$, which indicates that, at the departure time, the spacecraft is not thrusting. Therefore, the first section of the trajectory is unnecessary: the optimal trajectory begins when the spacecraft uses thrust for the first time. The departure time can be then postponed until the Switching Function is positive;

- $S_F(t_f) < 0$ which indicates that, at the arrival time, the spacecraft is not thrusting. This means that the final segment of the trajectory is a pointless

coasting arch, thus with no propulsion. The arrival time can be then anticipated until the Switching Function is positive.

These two factors are taken into account, and the solutions obtained are refined by adapting the initial and final times to achieve optimal mission duration.
These modifications are clearly linked to small or null changes in the payload fraction, as they simply imply the removal of unnecessary portions of the trajectory.

Figure (6.2) shows an example of the outcome of this analysis, for a single-target mission. The revised solution, as previously noted, presents a postponed departure time, an anticipated arrival time (resulting in a lower mission duration), and no ΔV modification, with respect to the initial solution.

Initial Solution	
Duration	ΔV [Km/s]
18.26	4.51

| Revised Solution	
Duration	ΔV [Km/s]
12.57	4.51
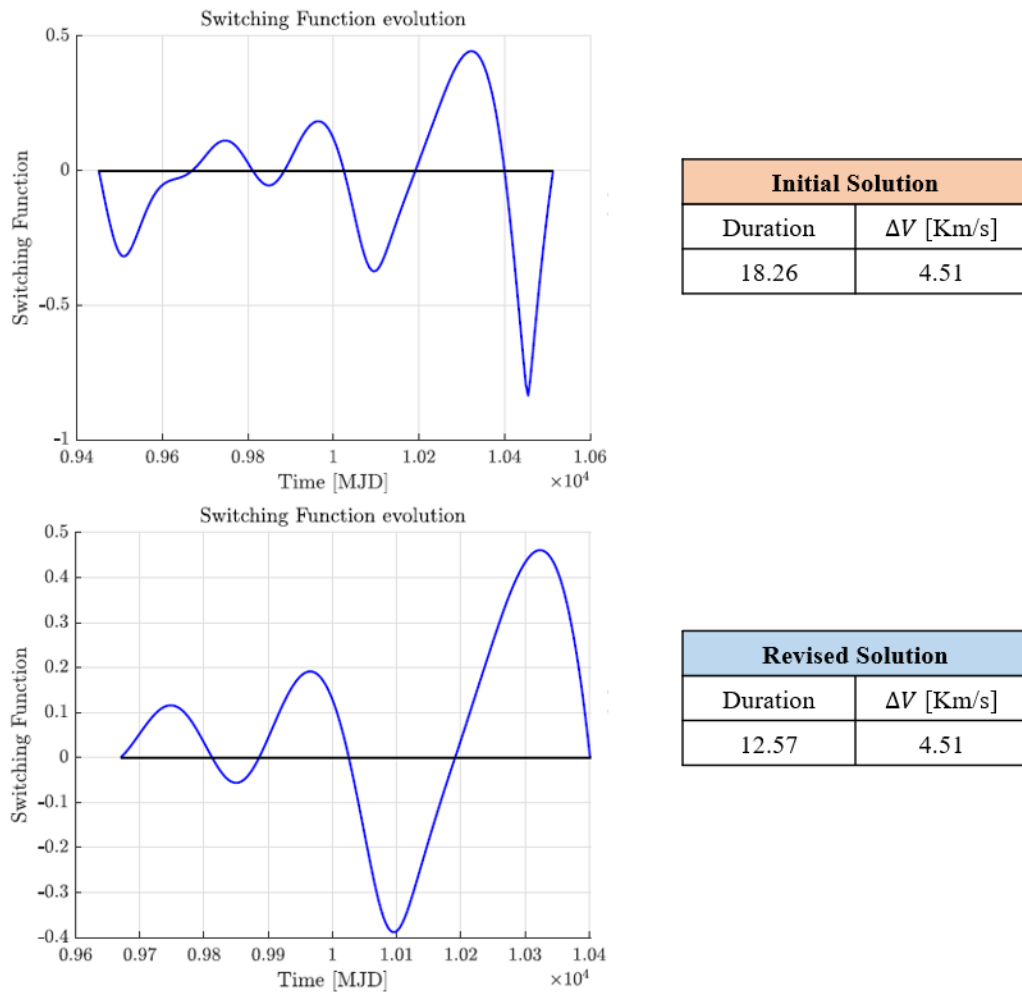
Figure 6.2: Correction of a single-target mission based on the Switching Function analysis

Chapter 7

Results

In this Chapter the results obtained from the trajectory optimization towards asteroids are presented. Near-Earth Numbered and Unnumbered Asteroids are considered as potential targets (whose orbital elements are available on JPL small-body elements database).
Among these targets, four specific asteroids (Table 7.1), particularly relevant from a scientific point of view, will be highlighted.

Asteroid
2009 CV
2013 WA44
2014 YD
2018 LQ2

Table 7.1: List of Asteroids recommended for scientific relevance

Before entering the particulars of the solutions, the architecture of this chapter is explained.
The first section focuses on optimal missions towards a single target. Sections two and three illustrate missions towards two and three targets, respectively.
For each mission, the following features are taken into account:

- orbital elements of the involved asteroids;

- asteroid's $\Delta\theta$ with respect to the Earth at arrival date;

- departure, arrival date and duration;

- ΔV for the entire mission;

- satellite's final mass.

Final masses and duration are expressed dimensionless.

For each section, different plots highlighting key aspects of the most interesting missions are showed. These plots, in particular, depict:

- satellite trajectory projected on the $x - y$ plane, to analyse the spacecraft's specific path. A bidimensional plot was chosen due to the low orbit inclination of the involved celestial bodies ($< 5°$);

- aphelion and perihelion distance profiles, to investigate how the mission is carried out and whether the phase shift angle $\Delta\theta$ between Earth and the target asteroid is optimal;

- semi-major axis and eccentricity profiles;

- Switching Function and thrust profiles, to evaluate the propelled and coasting portions of the mission.

It is worth noting that the correction based on the Switching Function, provided in section 6.4, has been adopted for each mission.

7.1 One-target missions

Missions from Earth to a final target are presented in this section. Those listed on Table 7.2 have Numbered asteroids as a target. The following ones, listed on Table 7.4, consider the asteroids recommended for scientific relevance (Table 7.1) as a target.

Mission n°	Asteroid	Departure Date	Arrival Date	Duration	ΔV (km/s)	m_f
1	2012 UV136	19/12/2027	14/12/2029	12.50	2.7631	0.9303
2	Apophis	23/6/2026	23/6/2028	12.57	4.5131	0.8887
3	2014 EK24	19/1/2025	12/4/2027	14.00	3.6556	0.9088
4	1996 XB27	10/5/2026	8/2/2028	11.00	3.3710	0.9156

Table 7.2: One-target missions towards Numbered Asteroids

Mission n°	Asteroid	a (AU)	e	i (deg)	ω (deg)	Ω (deg)	$\Delta\theta$ (deg)
1	2012 UV136	1.0073	0.1392	2.2134	288.6072	209.9000	65.6648
2	Apophis	0.9224	0.1911	3.3409	126.6732	203.89909	39.00
3	2014 EK24	1.0081	0.0701	4.8049	63.7473	340.5876	47.2332
4	1996 XB27	1.1888	0.0578	2.4645	58.1817	179.4123	52.8226

Table 7.3: One-target missions towards Numbered Asteroids: orbital elements and $\Delta\theta$

7.1.1   Focus on mission towards asteroid Apophis
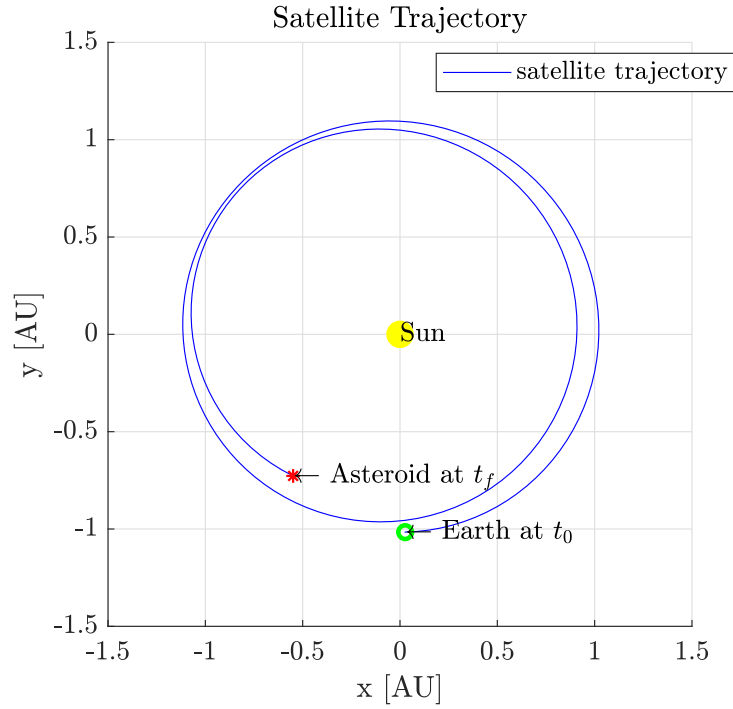

**Figure 7.1:** Two-dimensional satellite trajectory towards Asteroid 2013 WA44
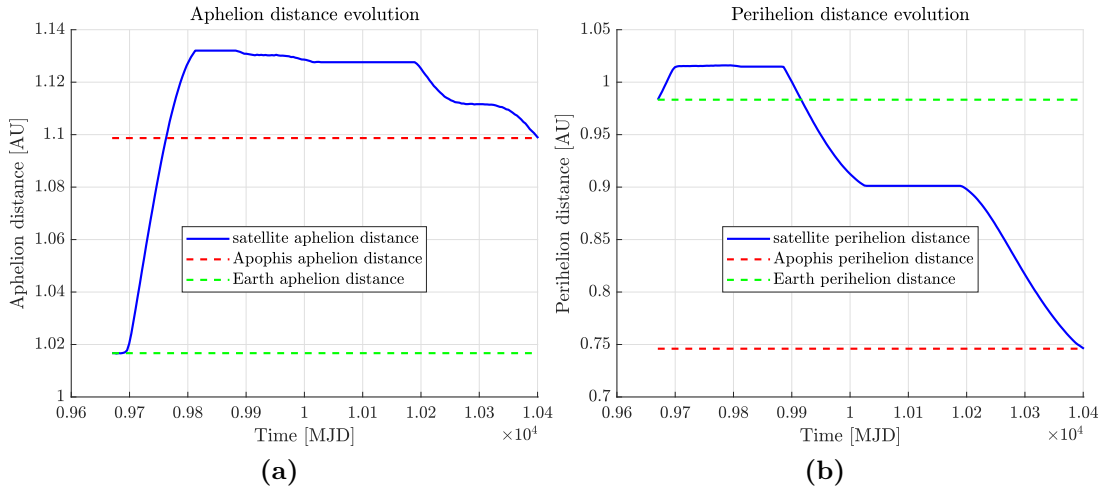
**Figure 7.2:** (a) Aphelion distance temporal evolution. (b) Perihelion distance temporal evolution

.
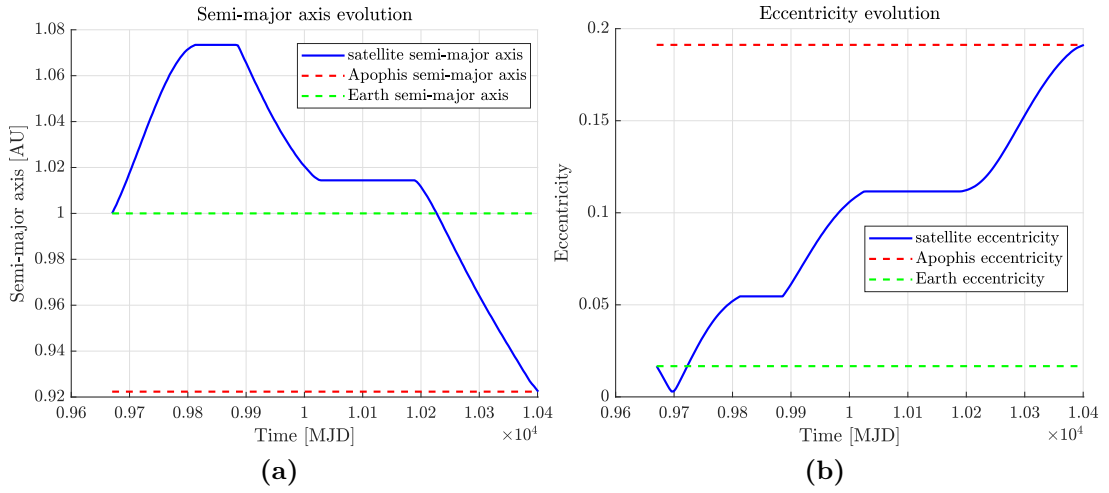
Figure 7.3: (a) Semi-major axis temporal evolution. (b) Eccentricity temporal evolution

.
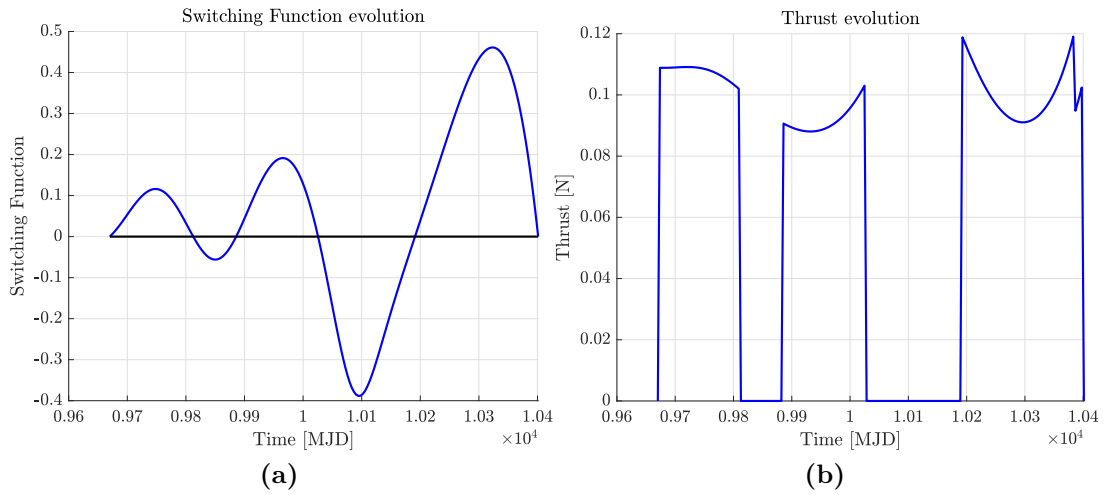
Figure 7.4: (a) Switching function temporal evolution. (b) Thrust temporal evolution

.

7.1.2   One-target missions (Asteroids from Table 7.1)

Mission n°	Asteroid	Departure Date	Arrival Date	Duration	ΔV (km/s)	m_f
5	2009 CV	19/9/2027	23/6/2029	11.06	2.6012	0.9342
6	2013 WA44	15/4/2028	13/8/2029	8.34	1.9051	0.9514
7	2014 YD	24/7/2033	7/7/2035	12.25	1.8399	0.9530
8	2018 LQ2	27/11/2032	6/11/2034	12.20	2.3230	0.9411

Table 7.4: One-target missions towards Asteroids from Table 7.1

Mission n°	Asteroid	a (AU)	e	i (deg)	ω (deg)	Ω (deg)	$\Delta\theta$ (deg)
5	2009 CV	1.1158	0.1508	0.9426	181.3443	22.3980	10.4338
6	2013 WA44	1.0975	0.0580	2.2993	177.5719	55.9866	15.2792
7	2014 YD	1.0721	0.0867	1.7359	34.1325	117.6397	4.1927
8	2018 LQ2	1.0911	0.0576	2.1260	142.8416	178.3061	10.4987

Table 7.5: One-target missions towards Asteroids from Table 7.1: orbital elements and $\Delta\theta$

### 7.1.3   Focus on mission towards asteroid 2013 WA44
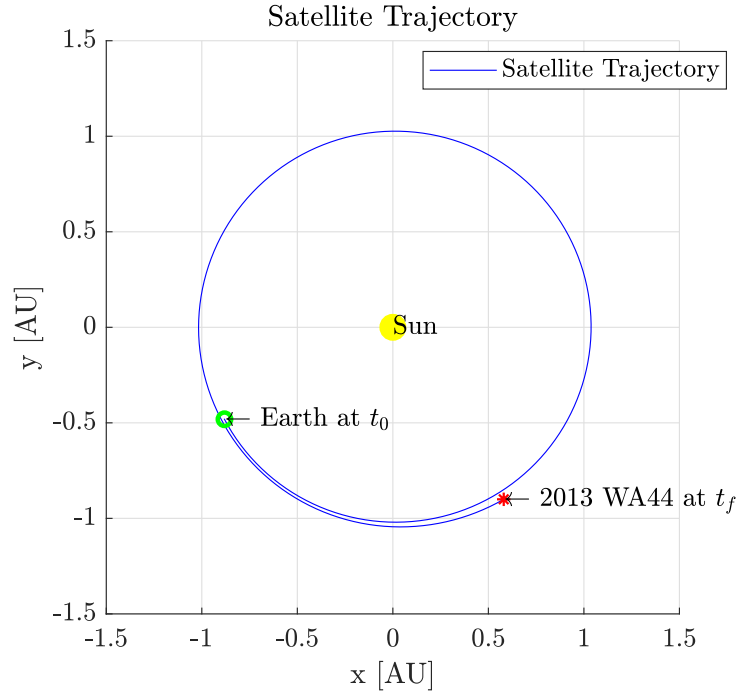
**Figure 7.5:** Two-dimensional satellite trajectory towards Asteroid 2013 WA44
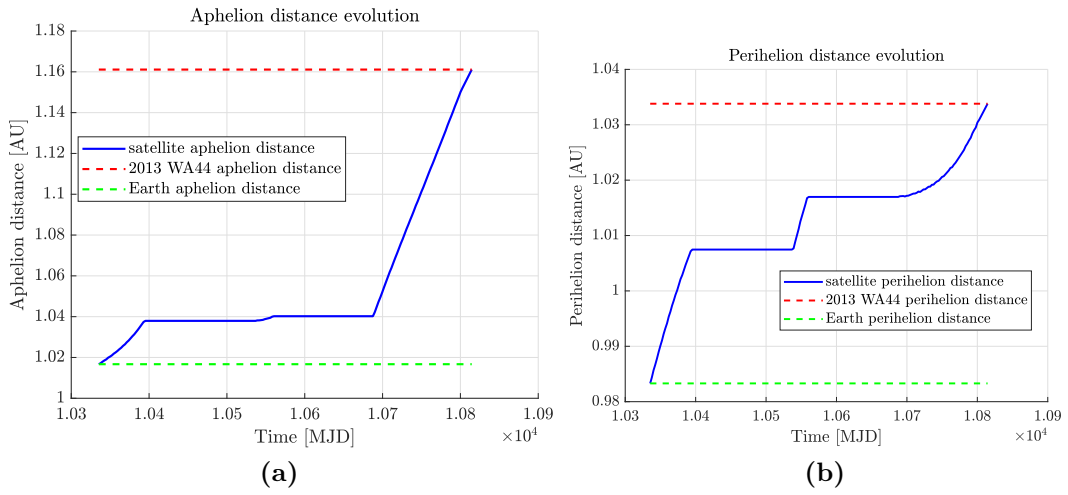
Figure 7.6: (a) Aphelion distance temporal evolution. (b) Perihelion distance temporal evolution

.
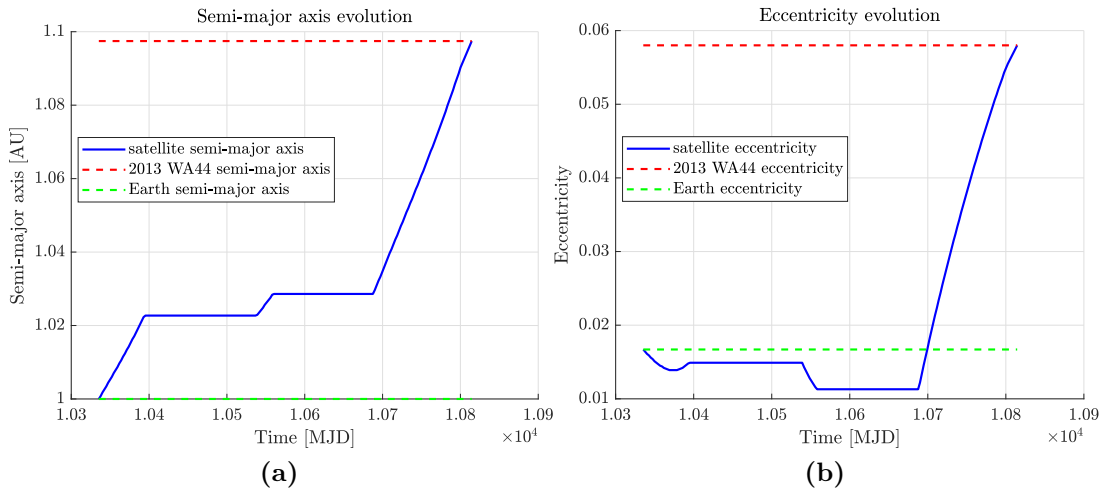
**Figure 7.7:** (a) Semi-major axis temporal evolution. (b) Eccentricity temporal evolution

.
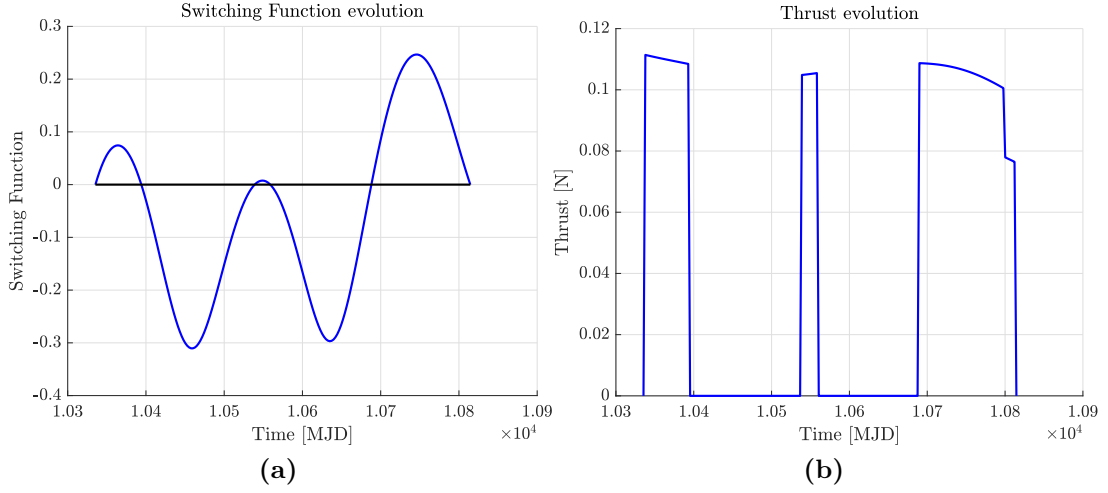
Figure 7.8: (a) Switching function temporal evolution. (b) Thrust temporal evolution

.

7.2 Two-target missions

This section considers two-target missions: before reaching the final body, the spacecraft performs a rendezvous manoeuvre with an *intermediate* asteroid. Solutions listed on Tables 7.6 and 7.8 have Unnumbered asteroids as a target. Table 7.10 reports missions involving at least one of the asteroids from Table 7.1 as a target.

Mission n°	1	2	3	4
Intermediate Asteroid	2000 SG344	2015 KK57	2012 WR10	2020 PC
Final Asteroid	2015 VC2	2020 GE	2020 OK5	2018 BC
Departure Date	13/3/2028	2/6/2030	30/3/2028	30/12/2028
Arrival Date to Int.	26/11/2028	13/10/2031	31/10/2029	13/1/2030
Arrival Date to Final	23/1/2031	20/10/2032	13/12/2030	18/7/2031
Duration	18.00	15.75	17.00	16.00
$\mathbf{\Delta V_{tot}}$ **(km/s)**	2.5230	3.6570	3.7147	3.8881
$\mathbf{\Delta V_{01}}$ **(km/s)**	1.2056	2.1226	1.9626	1.4602
$\mathbf{\Delta V_{12}}$ **(km/s)**	1.3173	1.5344	1.7521	2.4279
$\mathbf{m_f}$	0.9361	0.9088	0.9074	0.9033

Table 7.6: Two-target missions towards Unnumbered Asteroids (1)

Mission n°1	a (AU)	e	i (deg)	ω (deg)	Ω (deg)	$\Delta\theta$ (deg)
2000 SG344	0.9773	0.0668	0.1123	275.4000	191.8592	3.3360
2015 VC2	1.0530	0.0744	0.8679	288.2665	186.1519	49.5078

Mission n°2	a (AU)	e	i (deg)	ω (deg)	Ω (deg)	$\Delta\theta$ (deg)
2015 KK7	1.0918	0.0636	1.0319	100.0849	194.4045	8.3298
2020 GE	1.0057	0.0394	2.2842	109.4423	181.1617	25.2137

Mission n°3	a (AU)	e	i (deg)	ω (deg)	Ω (deg)	$\Delta\theta$ (deg)
2012 WR10	1.0853	0.1116	0.3078	146.9155	224.1384	14.1677
2020 OK5	1.0806	0.0836	1.0064	108.1034	295.8514	40.0720

Mission n°4	a (AU)	e	i (deg)	ω (deg)	Ω (deg)	$\Delta\theta$ (deg)
2020 PC	0.9331	0.0957	0.3207	241.4705	228.0415	19.3037
2018 BC	1.0483	0.0697	2.8644	212.8001	297.2204	33.0187

Table 7.7: Two-target missions towards Unnumbered Asteroids (1): orbital elements and $\Delta\theta$

Mission n°	5	6	7	8
Intermediate Asteroid	2019 WS3	2011 BL45	2018 GR4	2018 FM2
Final Asteroid	2020 DG3	2019 WS3	2015 VC2	2015 VC2
Departure Date	24/1/2030	18/7/2028	15/4/2027	14/6/2027
Arrival Date to Int.	19/4/2031	20/9/2029	9/5/2028	19/8/2028
Arrival Date to Final	18/4/2032	23/1/2031	28/12/2029	11/3/2030
Duration	14.02	17.87	17.00	17.22
ΔV_{tot} (km/s)	4.4515	4.6031	5.4737	5.5619
ΔV_{01} (km/s)	2.1540	1.9771	1.9579	2.4026
ΔV_{12} (km/s)	2.2975	2.6260	3.5158	3.1593
m_f	0.8901	0.8866	0.8666	0.8646

Table 7.8: Two-target missions towards Unnumbered Asteroids (2)

Mission n°5	a (AU)	e	i (deg)	ω (deg)	Ω (deg)	Δθ (deg)
2019 WS3	1.063	0.0861	1.9162	188.6622	164.1394	15.0149
2020 DG3	1.0608	0.0934	2.9113	287.6100	157.9154	11.7221

Mission n°6	a (AU)	e	i (deg)	ω (deg)	Ω (deg)	Δθ (deg)
2011 BL45	1.0918	0.0636	1.0319	100.0849	194.4045	5.3529
2019 WS3	1.0631	0.0861	1.9162	188.6623	164.1394	4.7837

Mission n°7	a (AU)	e	i (deg)	ω (deg)	Ω (deg)	Δθ (deg)
2018 GR4	0.9360	0.1110	1.0043	232.8821	167.5899	9.4521
2015 VC2	1.0530	0.0744	0.8679	288.2665	186.1519	19.4625

Mission n°8	a (AU)	e	i (deg)	ω (deg)	Ω (deg)	Δθ (deg)
2018 FM2	0.9418	0.0946	1.1580	191.9393	143.0572	3.9319
2015 VC2	1.0530	0.0744	0.8679	288.2665	186.1519	16.6776

Table 7.9: Two-target missions towards Unnumbered Asteroids (2): orbital elements and $\Delta\theta$

7.2.1 Focus on mission n°1
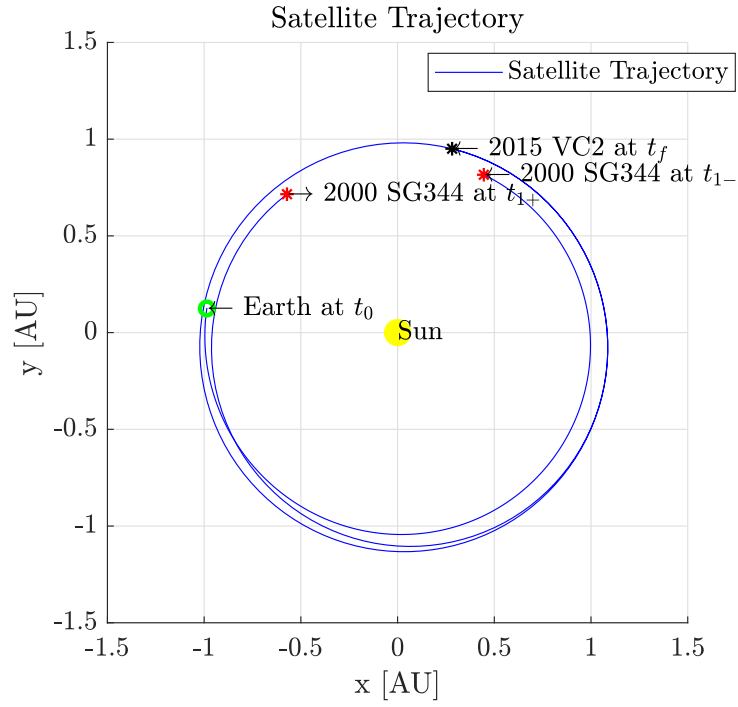

Figure 7.9: Two-dimensional satellite trajectory
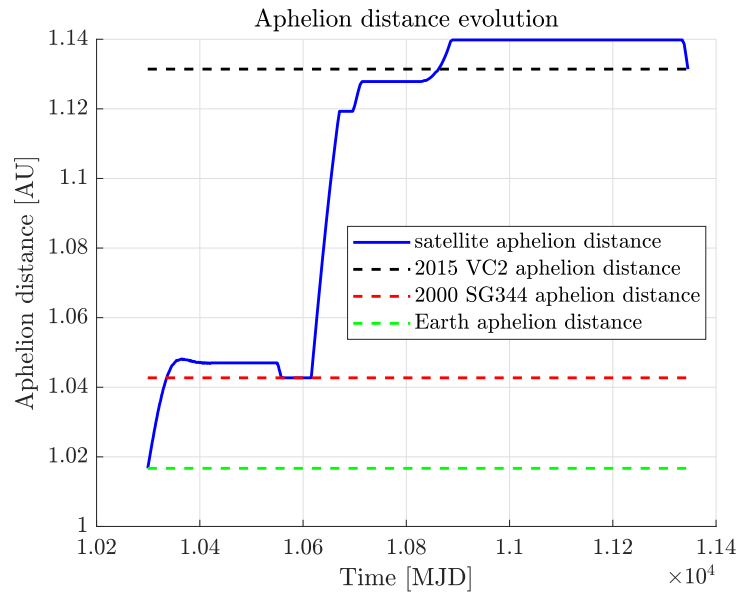

Figure 7.10: Aphelion distance temporal evolution
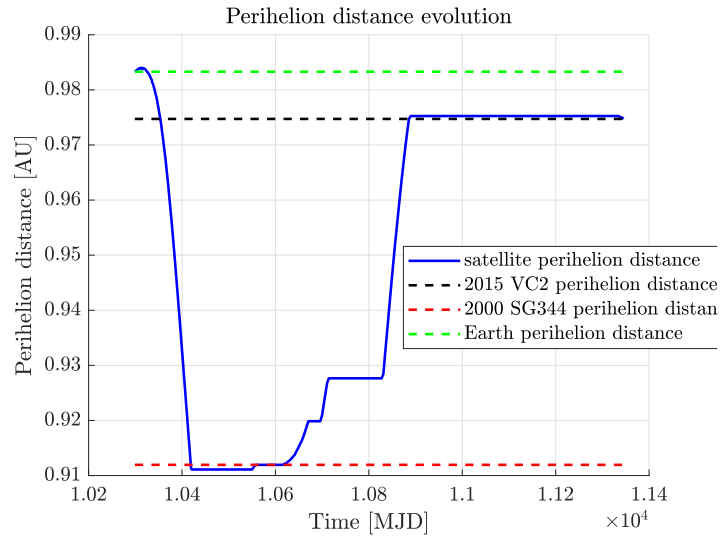
Figure 7.11: Perihelion distance temporal evolution
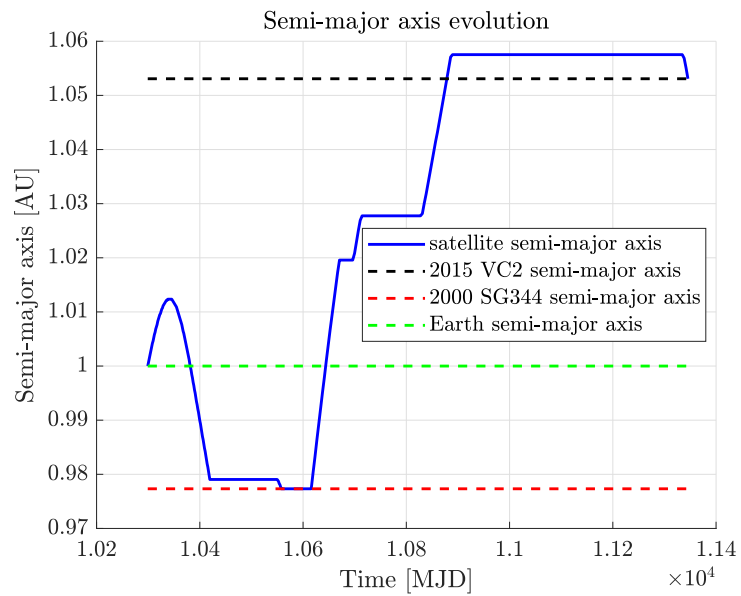

Figure 7.12: Semi-major axis temporal evolution

67
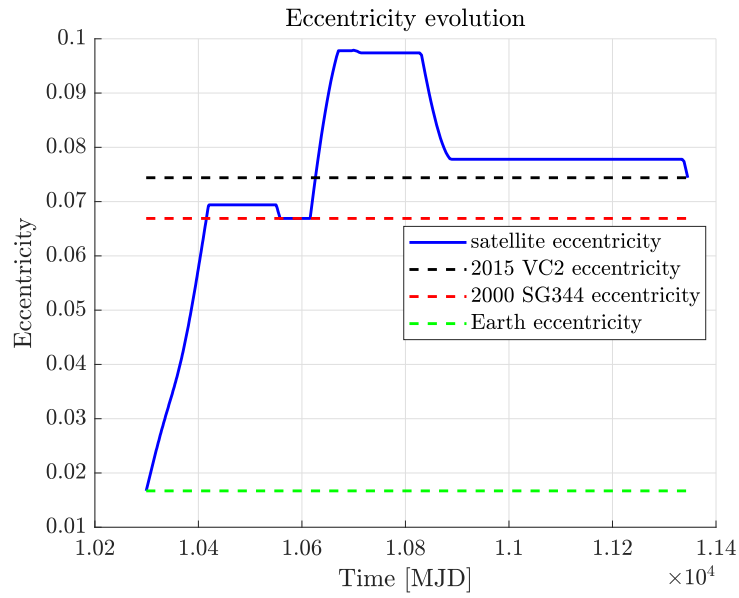
Figure 7.13: Eccentricity temporal evolution
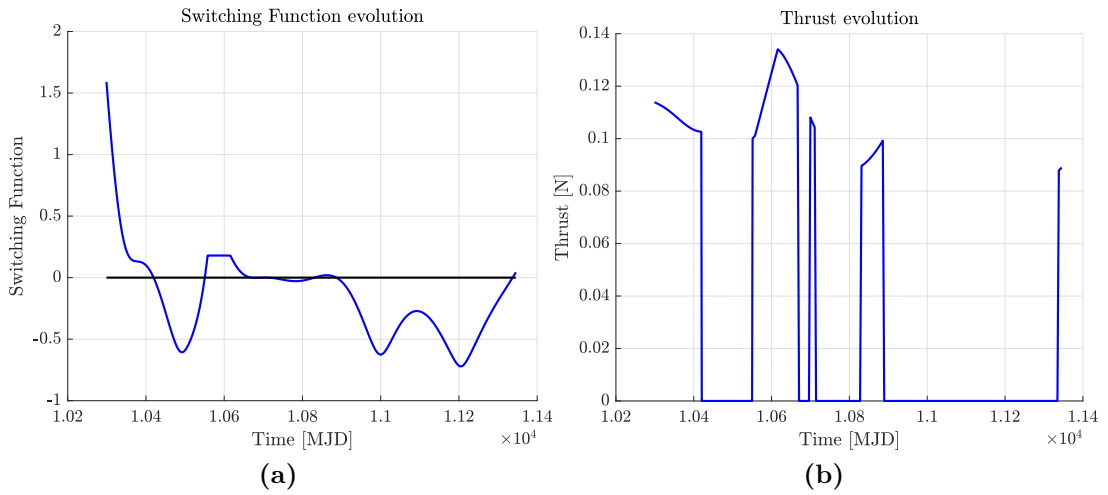
Figure 7.14: (a) Switching temporal function evolution. (b) Thrust temporal evolution

.

7.2.2   Focus on mission n°5
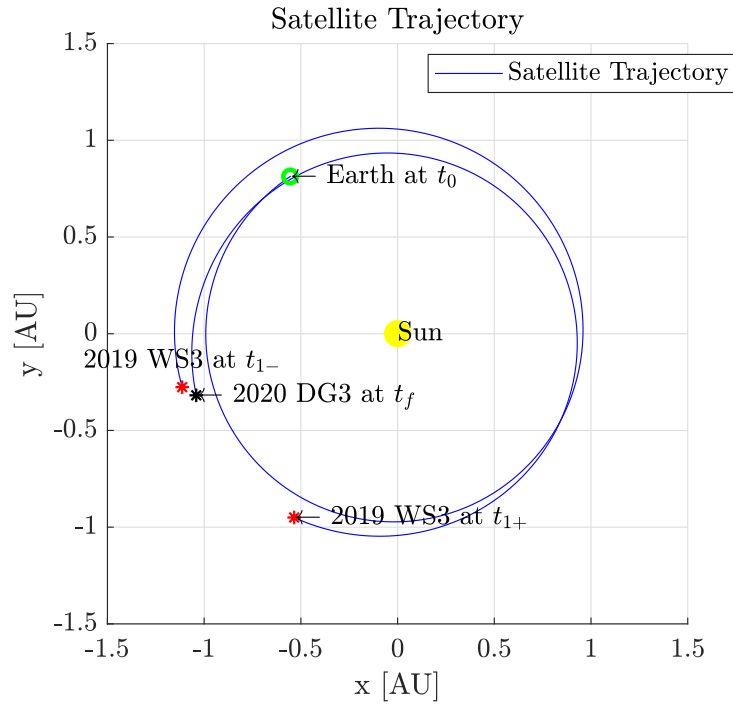
**Figure 7.15:** Two-dimensional satellite trajectory
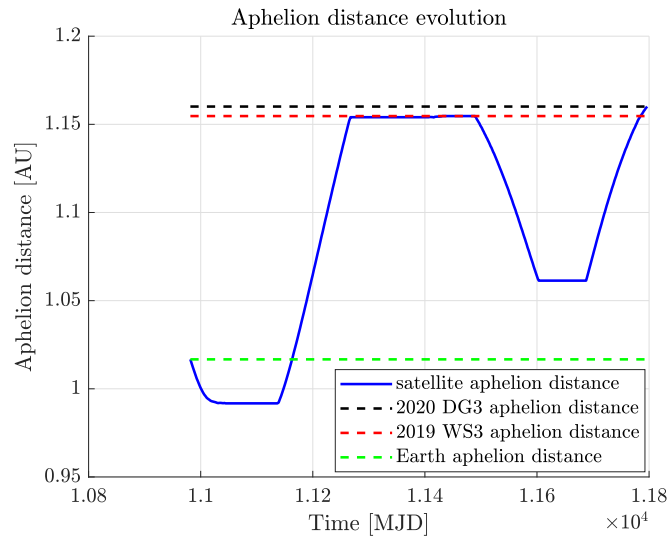
**Figure 7.16:** Aphelion distance temporal evolution
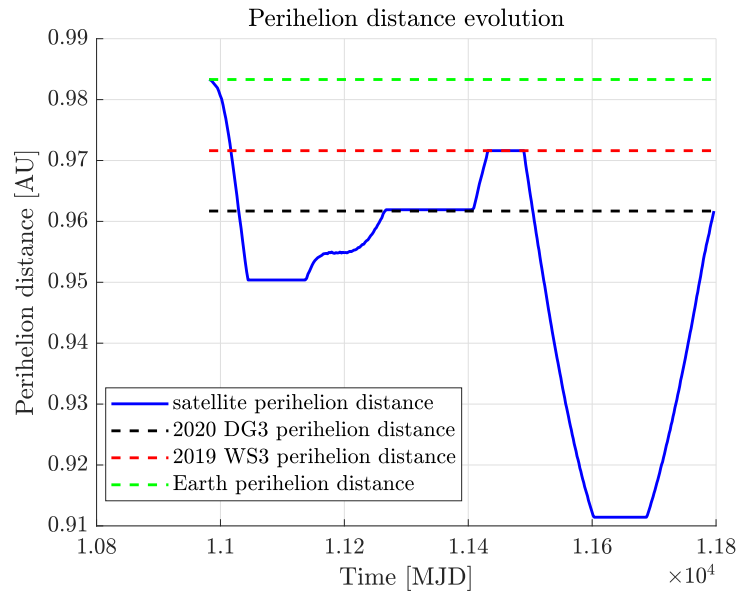
**Figure 7.17:** Perihelion distance temporal evolution
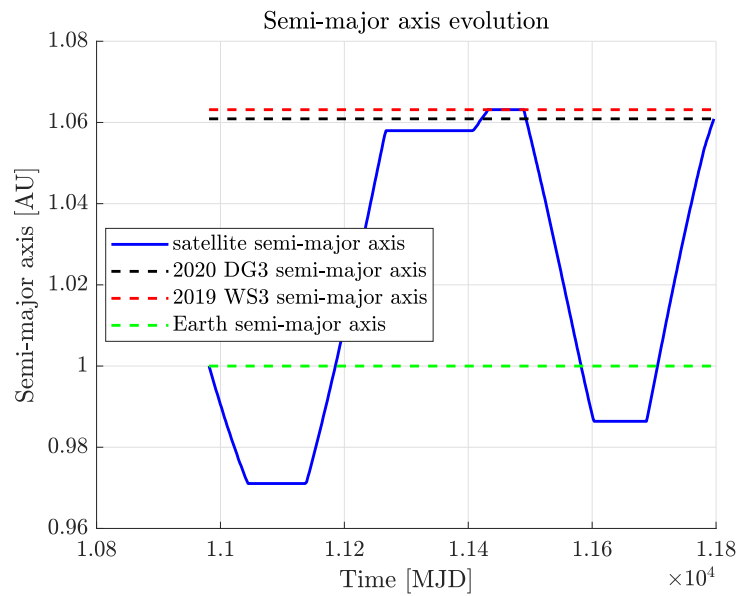

Figure 7.18: Semi-major axis temporal evolution
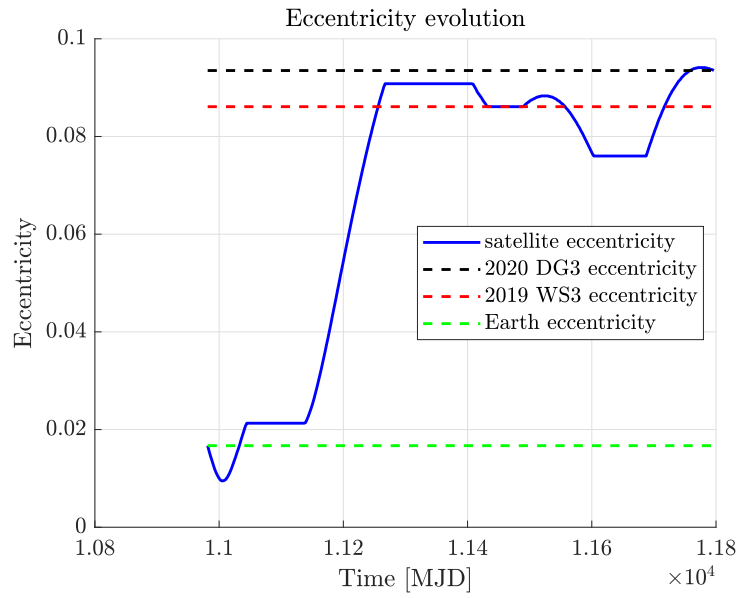
Figure 7.19: Eccentricity temporal evolution
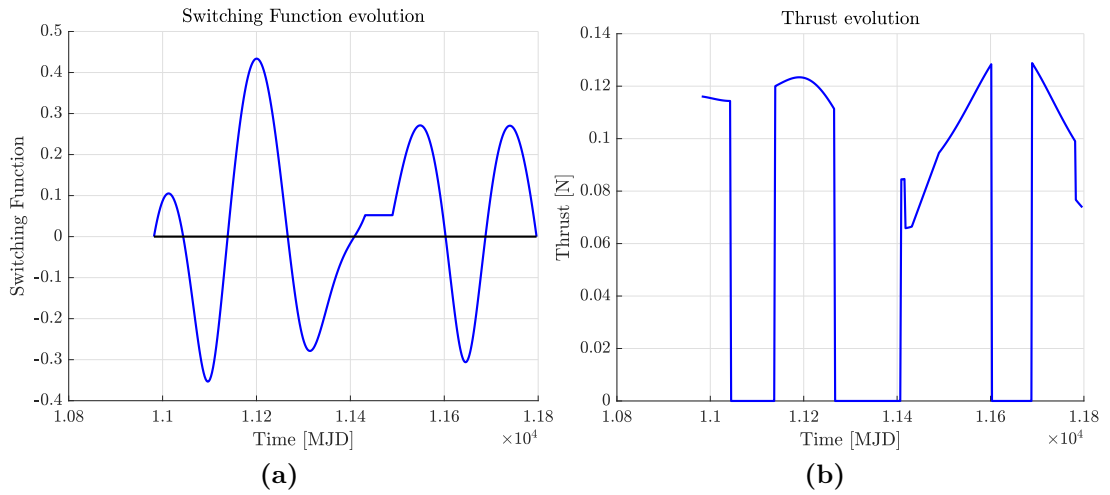
Figure 7.20: (a) Switching function temporal evolution. (b) Thrust temporal evolution

.

71

7.2.3 Two-target missions (Asteroids from Table 7.1)

Mission n°	9	10	11	12
Intermediate Asteroid	2013 WA44	2017 UQ6	2021 WV1	2010 JK1
Final Asteroid	2009 CV	2013 WA44	2014 YD	2018 LQ2
Departure Date	6/6/2026	30/1/2027	20/6/2032	12/12/2032
Arrival Date to Int.	19/6/2028	30/5/2028	26/3/2034	27/10/2033
Arrival Date to Final	29/4/2029	14/10/2029	3/4/2035	24/5/2035
Duration	18.20	17.00	17.50	15.37
$\mathbf{\Delta V_{tot}}$ **(km/s)**	6.0266	5.6557	3.9713	4.7449
$\mathbf{\Delta V_{01}}$ **(km/s)**	3.8403	2.8839	3.0222	2.9431
$\mathbf{\Delta V_{12}}$ **(km/s)**	2.1862	2.7718	0.9491	1.8018
$\mathbf{m_f}$	0.8542	0.8625	0.9013	0.8833

Table 7.10: Two-target missions towards Asteroids from Table 7.1

Mission n°9	a (AU)	e	i (deg)	ω (deg)	Ω (deg)	$\Delta\theta$ (deg)
2013 WA44	1.0975	0.0579	2.2992	177.5719	55.9866	36.9852
2009 CV	1.1158	0.1508	0.9426	181.3443	22.3980	6.6793

Mission n°10	a (AU)	e	i (deg)	ω (deg)	Ω (deg)	$\Delta\theta$ (deg)
2017 UQ6	0.9438	0.1097	0.5906	229.7608	333.3628	7.8268
2013 WA44	1.0975	0.0579	2.2992	177.5719	55.9866	23.1423

Mission n°11	a (AU)	e	i (deg)	ω (deg)	Ω (deg)	$\Delta\theta$ (deg)
2021 WV1	1.0526	0.1064	1.7896	54.0210	82.6199	52.2265
2014 YD	1.0721	0.0867	1.7359	34.1325	117.6397	12.0319

Mission n°12	a (AU)	e	i (deg)	ω (deg)	Ω (deg)	$\Delta\theta$ (deg)
2010 JK1	1.0294	0.1504	0.1671	137.8724	201.7821	38.6009
2018 LQ2	1.0911	0.0576	2.1260	142.8416	178.3061	29.4530

Table 7.11: Two-target missions towards Asteroids from Table 7.1: orbital elements and $\Delta\theta$

7.2.4   Focus on mission n°9
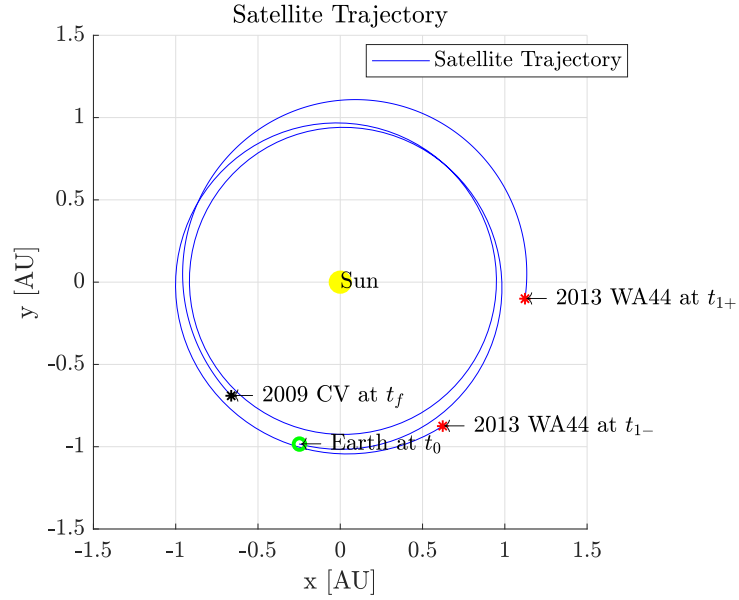
**Figure 7.21:** Two-dimensional satellite trajectory
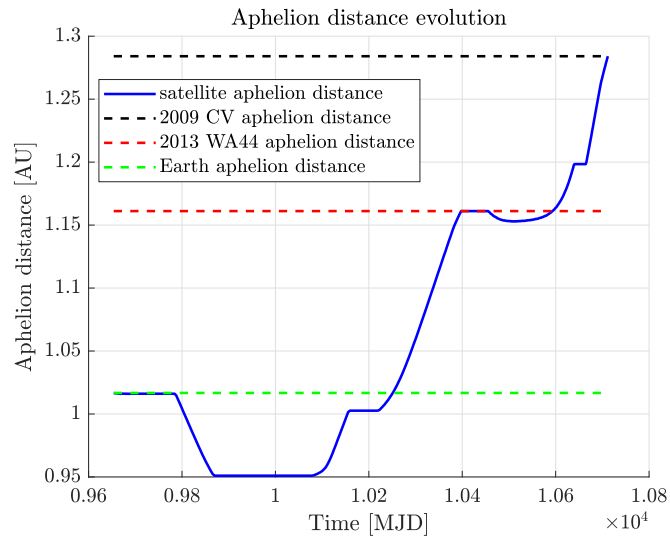
**Figure 7.22:** Aphelion distance temporal evolution
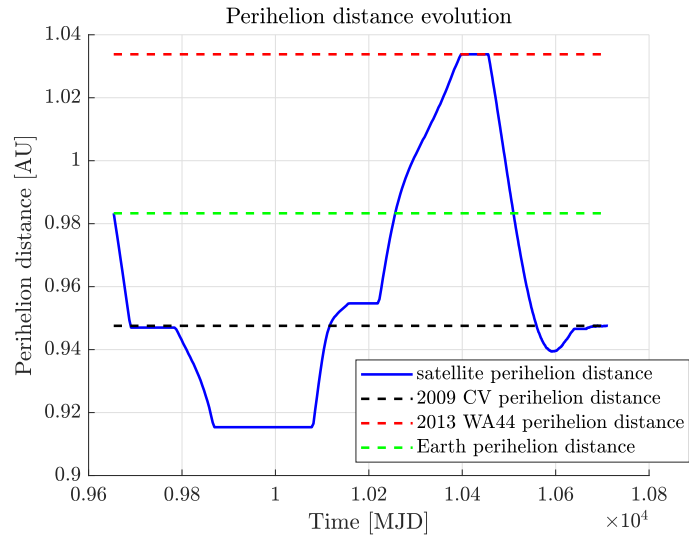
Figure 7.23: Perihelion distance temporal evolution
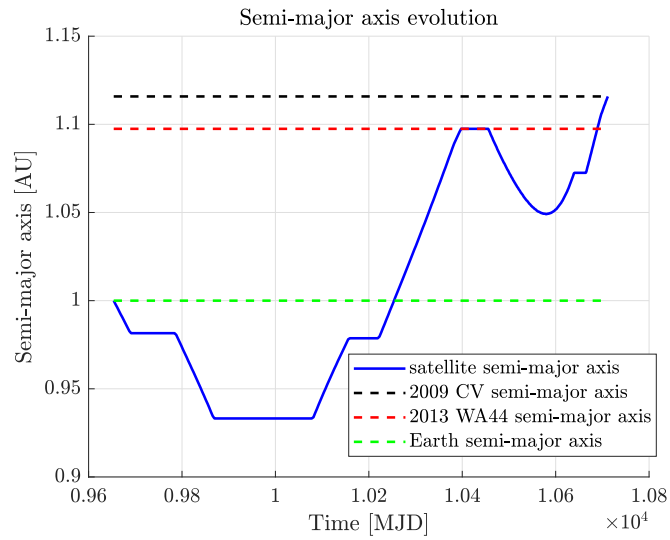
**Figure 7.24:** Semi-major axis temporal evolution
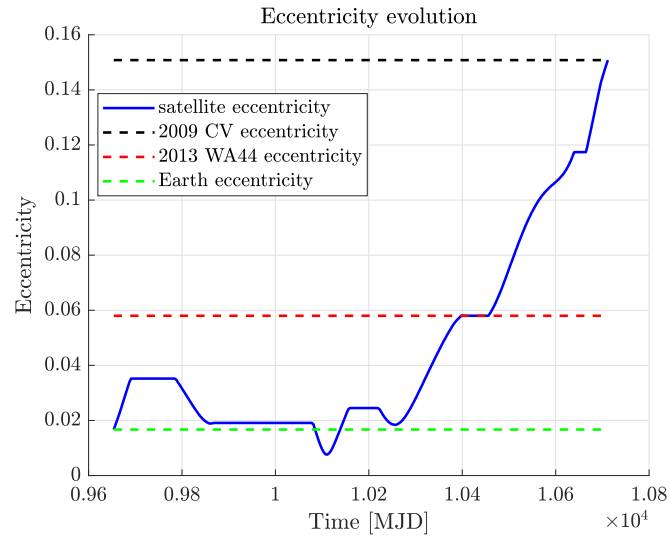
Figure 7.25: Eccentricity temporal evolution
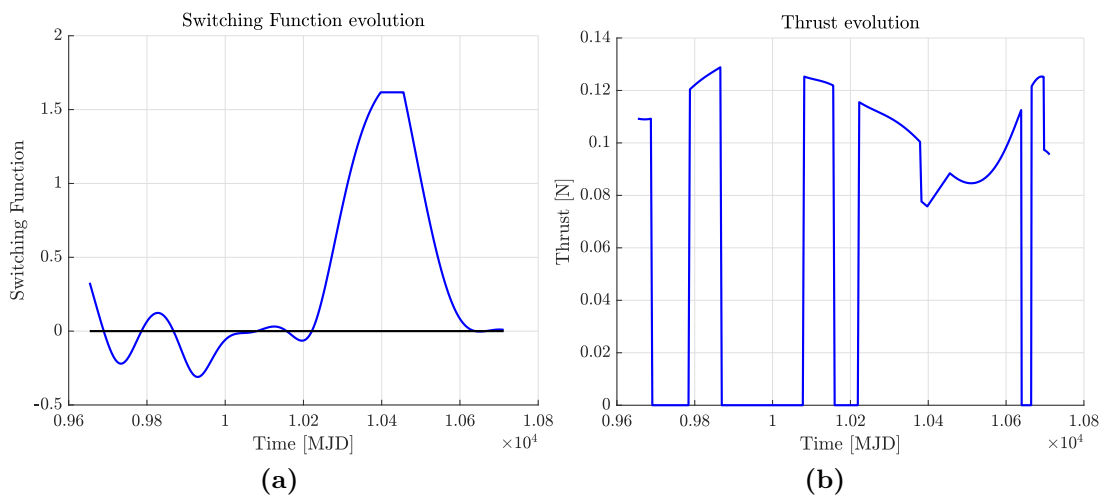

Figure 7.26: (a) Switching function temporal evolution. (b) Thrust temporal evolution

.

7.3 Three-target missions

This section considers three-target missions: before reaching the final body, the spacecraft performs rendezvous manoeuvres with two *intermediate* asteroids.

Mission n°	1	2	3
First intermediate Asteroid	2015 KK57	2014 HN2	2017 FB3
Second intermediate Asteroid	2020 GE	2014 WX202	2015 NA14
Final Asteroid	2020 XH2	2009 HE60	2006 FH36
Departure Date	30/9/2030	24/11/2029	18/4/2030
Arrival Date to First Int.	18/10/2031	17/3/2031	21/6/2031
Arrival Date to Second Int.	20/11/2032	19/4/2032	20/10/2032
Arrival Date to Final	29/4/2034	6/10/2033	6/3/2034
Duration	22.50	24.30	24.40
ΔV_{tot} (km/s)	6.4184	8.8816	10.8949
ΔV_{01} (km/s)	2.1074	2.2897	3.2142
ΔV_{12} (km/s)	1.5557	2.1903	4.0858
ΔV_{23} (km/s)	2.7552	4.4015	3.5948
m_f	0.8455	0.7927	0.7521

Table 7.12: Three-target missions towards Unnumbered Asteroids

Mission n°1	a (AU)	e	i (deg)	ω (deg)	Ω (deg)	$\Delta\theta$ (deg)
2015 KK57	1.0917	0.0636	1.0319	100.0849	194.4045	7.5631
2020 GE	1.0057	0.0394	2.2842	109.4423	181.1617	25.8227
2020 XH2	0.9519	0.1922	1.0414	101.3832	218.3307	32.1063

Mission n°2	a (AU)	e	i (deg)	ω (deg)	Ω (deg)	$\Delta\theta$ (deg)
2014 HN2	0.9266	0.1184	1.2359	207.4161	198.8469	20.1467
2014 WX202	1.0355	0.0587	0.4127	214.1180	243.9468	43.3432
2009 HE60	0.9954	0.2644	1.5831	219.8236	228.9162	3.6163

Mission n°3	a (AU)	e	i (deg)	ω (deg)	Ω (deg)	$\Delta\theta$ (deg)
2017 FB3	1.0469	0.1863	1.0072	42.0314	291.0090	5.6452
2015 NA14	0.9661	0.1839	6.3534	152.8119	281.8254	32.8216
2006 FH36	0.9554	0.1982	1.5830	156.8977	278.1277	3.3620

Table 7.13: Three-target missions towards Unnumbered Asteroids: orbital elements and $\Delta\theta$

7.3.1 Focus on mission n°1
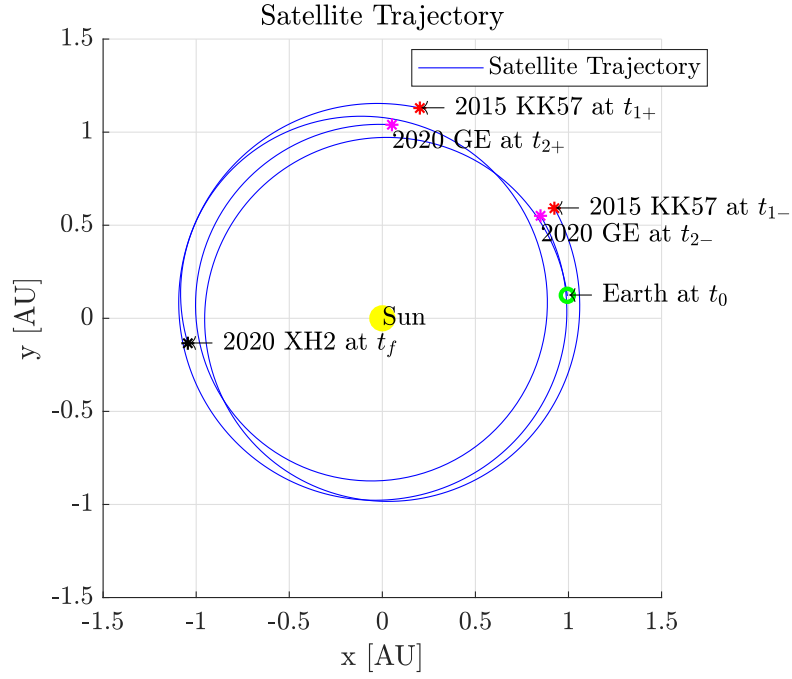
**Figure 7.27:** Two-dimensional satellite trajectory
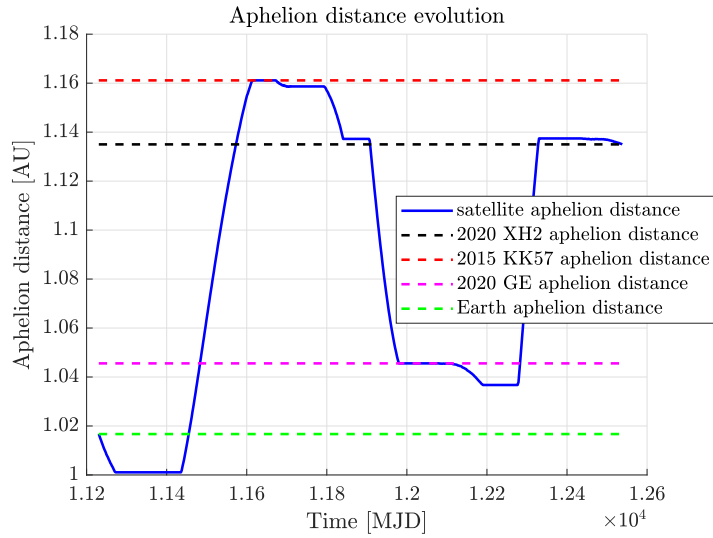
**Figure 7.28:** Aphelion distance temporal evolution
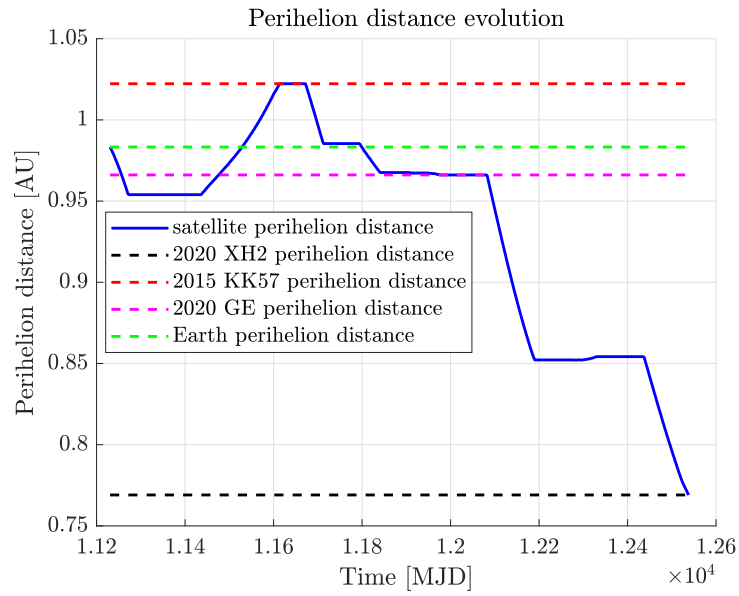
Figure 7.29: Perihelion distance temporal evolution
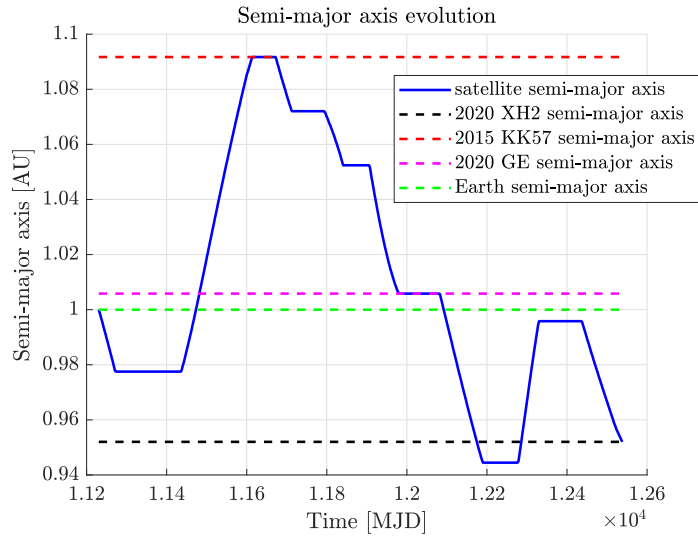
**Figure 7.30:** Semi-major axis temporal evolution
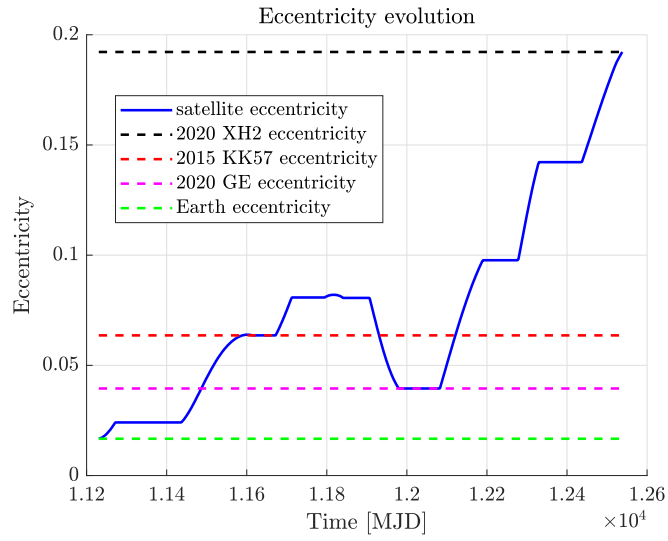
Figure 7.31: Eccentricity temporal evolution

**(a)**   **(b)**
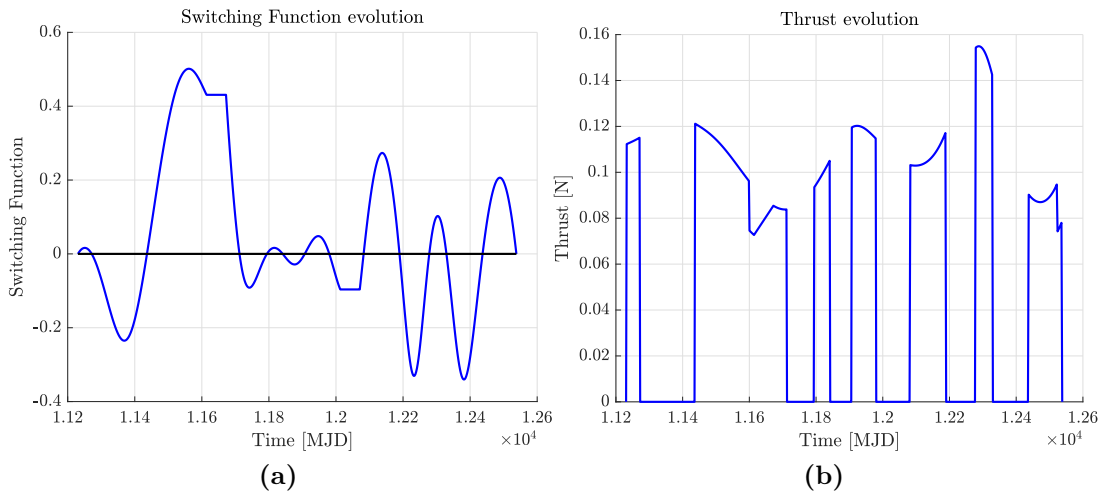
Figure 7.32: (a) Switching function temporal evolution. (b) Thrust temporal evolution

.

7.4   Results overview

Solutions provided in the previous sections validate the proposed procedures for defining initial guesses, allowing for a straightforward determination of optimized multiple rendezvous missions. Indeed, by starting the integration from the tentative solutions determined as mentioned in Section 6.3, the indirect method's convergence difficulties were successfully addressed, and solutions were easily obtained. Furthermore, the presented missions have interesting features. This section gives therefore an overview of the results, emphasizing the most relevant mission aspects. Two mission's attributes, in particular, are considered:

- mission's propulsive cost, expressed as its *characteristic velocity* ΔV, which is directly related to the spacecraft's final mass (as mentioned in section 3.2). The fraction of the spacecraft dedicated to propellant storage is influenced by the ΔV, and thus determines the mission's feasibility and scientific return;

- mission's duration, which should be kept to a minimum, for at least a couple of reasons:

  - to accomplish the mission's objectives as quickly as possible;
  - to reduce the interaction of the spacecraft with its orbital environment, since a variety of hazards are associated with the operation of spacecraft in the harsh space environment.

It is worth mentioning that, in general, mission's duration and propulsive cost are inversely related.
The overview of solutions is presented separately for missions to one, two, and three targets.

Results overview: one-target missions

Eight different one-target missions were presented. These missions have:

- missions' duration between 1 year and 4 months (Mission n° 6) and 2 years and 3 months (Mission n° 3).

- missions' ΔV between 1.84 km/s (Mission n° 7) and 4.51 km/s (Mission n° 2).

In particular, seven missions out of the eight presented show duration ≤ 2 years (the only exception is Mission n° 3); moreover five missions out of the eight presented show $\Delta V \leq 3$ km/s, and three of them show $\Delta V < 2.5$ km/s.
When both of the mission's features are taken into account, Mission n° 6 emerges as the best option, with a duration of 1 year and 4 months and a ΔV of 1.90 km/s.

Results overview: two-target missions

Twelve different two-target missions were presented. These missions have:

- missions' duration between 2 year and 3 months (Mission n° 5) and 2 years and 11 months (Mission n° 9).

- missions' ΔV_{tot} between 2.52 km/s (Mission n° 1) and 6.02 km/s (Mission n° 9).

In particular, eight missions out of the twelve presented show $\Delta V_{tot} < 5$ km/s, and three of them show $\Delta V_{tot} < 4$ km/s.
When both of the mission's features are taken into account, Mission n° 2 emerges as the best option, with a duration of 2 year and 6 months and a ΔV_{tot} of 3.65 km/s.

Results overview: three-target missions

Three different three-target missions were presented. These missions have:

- missions' duration between 3 year and 7 months (Mission n° 1) and 3 years and 11 months (Mission n° 3).

- missions' ΔV_{tot} between 6.42 km/s (Mission n° 1) and 10.89 km/s (Mission n° 3).

When both of the mission's features are taken into account, Mission n° 1 emerges as the best option, with a duration of 3 year and 7 months and a ΔV_{tot} of 6.42 km/s.

Chapter 8

Conclusions

The problem of trajectory optimization for the case of multiple Near-Earth Asteroids (NEAs) rendezvous missions, using electric propulsion has been investigated. The examined space missions, in particular, consider a spacecraft departing from Earth at t_0 and visiting N asteroids at different dates t_N, with at most $N = 3$. A departure window from 2025 to 2035 has been fixed. A rendezvous maneuver is carried out for each asteroid, with a stay of about two months. Given the relevance of these celestial bodies, highlighted in Chapter 2, during this period the spacecraft can potentially conduct analyses and investigations on asteroids. Cubesats deployment by the primary mission can be an alternative option, in order to provide additional data of the asteroids, exploiting the agility of small spacecrafts. Furthermore, demonstrating the utilisation of smallsat technologies in deep space should push the boundaries of the technology to achieve higher performance levels and improve reliability.

Only the heliocentric legs of the spacecraft trajectories are examined in this work: the spacecraft leaves the Earth's sphere of influence at the initial time with position and velocity coincident with the planet's values. At rendezvous with the target, position and velocity match the asteroid's values.

A numerical code that implements an indirect method using shooting techniques has been employed. This method provides exact and reliable solutions (within the limitations of mathematical modeling of the system's dynamics), but it is sensitive to the precision of the tentative solution. Thus, suitable procedures to estimate the initial guess and to obtain solutions rapidly for the cases of one, two, and three target missions have been discussed. In Chapter 7, various examples were presented to validate these procedures.

These solutions were quickly achieved and present interesting features, including:

- mission duration ≤ 2 years and $\Delta V \leq 3$ km/s for single-target missions;

- mission duration ≤ 3 years and $\Delta V_{tot} \leq 5$ km/s, for two-target missions;

- mission duration $\leq$ 4 years and $\Delta V_{tot} \leq 10$ km/s, for three-target missions;

As a result, the proposed procedures are simple to implement, allow to overcome convergence difficulties, and produce good outcomes in terms of mission characteristics.

Future advances of this work may include:

- analysis of missions targeting at asteroids not included in this study. Indeed, not all of the potential targets have been examined. Moreover, new NEAs discoveries are continuously expanding the number of potential targets;

- analysis of the spacecraft trajectory once the rendezvous maneuver has been performed. Indeed, the evaluation of close operations required to examine the asteroid's characteristics, or necessary to deflect its orbit, could be of interest.

Bibliography

[1] Abolfazl Shirazi, Josu Ceberio, and Jose Lozano. «Spacecraft trajectory optimization: A review of models, objectives, approaches and solutions». In: *Progress in Aerospace Sciences* 102 (Aug. 2018).

[2] Bruce A. Conway. «The Problem of Spacecraft Trajectory Optimization». In: *Spacecraft Trajectory Optimization*. Ed. by Bruce A.Editor Conway. Cambridge Aerospace Series. Cambridge University Press, 2010, pp. 1–15.

[3] D. F. Lawden. *Optimal Trajectories for Space Navigation*. Butterworths mathematical texts. Butterworths, 1963.

[4] Mischa Kim. «Continuous low-thrust trajectory optimization: techniques and applications». PhD thesis. Virginia Polytechnic Institute and State University, 2005.

[5] Guido Colasurdo and Lorenzo Casalino. «Indirect Methods for the Optimization of Spacecraft Trajectories». In: *Modeling and Optimization in Space Engineering*. Ed. by Giorgio Fasano and János D. Pintér. New York, NY: Springer New York, 2013, pp. 141–158.

[6] Centre for Near-Earth Object studies NASA JPL. *Near Earth Objects, Basics*. URL: https://cneos.jpl.nasa.gov/about/basics.html.

[7] Lucy A. McFadden and Richard P. Binzel. «CHAPTER 14 - Near-Earth Objects». In: *Encyclopedia of the Solar System (Second Edition)*. Ed. by Lucy-Ann McFadden, Paul R. Weissman, and Torrence V. Johnson. Second Edition. San Diego: Academic Press, 2007, pp. 283–300.

[8] Near-Earth Object Coordination Centre ESA. *Discovery Statistics*. URL: https://neo.ssa.esa.int/discovery-statistics.

[9] Centre for Near-Earth Object studies NASA JPL. *Discovery Statistics*. URL: https://cneos.jpl.nasa.gov/stats/totals.html.

[10] D. S. Lauretta et al. «OSIRIS-REx: Sample Return from Asteroid (101955) Bennu». In: *Space Science Reviews* 212 (Aug. 2017), pp. 925–984.

[11] Donald K. Yeomans NASA JPL. *Why Study Asteroids?* 1998. URL: https://ssd.jpl.nasa.gov/sb/why_asteroids.html.

[12] Niklas Anthony and M. Reza Emami. «Asteroid engineering: The state-of-the-art of Near-Earth Asteroids science and technology». In: *Progress in Aerospace Sciences* 100 (2018), pp. 1–17.

[13] R.R. Bate, D.D. Mueller, and J.E. White. *Fundamentals of Astrodynamics.* Dover Books on Aeronautical Engineering Series. Dover Publications, 1971.

[14] H. Curtis. *Orbital Mechanics: For Engineering Students.* Aerospace Engineering. Elsevier Science, 2015.

[15] National Air and Smithsonian Institution Space Museum. *Rocket Propulsion.* URL: https://howthingsfly.si.edu/propulsion/rocket-propulsion.

[16] J.W. Cornelisse, H.F.R. Schöyer, and K.F. Wakker. *Rocket Propulsion and Spaceflight Dynamics.* Aerospace Engineering Series. Pitman, 1979. ISBN: 9780273011415.

[17] Lorenzo Casalino. *Generalities of Space Propulsion.* 2021.

[18] R.G. Jahn. *Physics of Electric Propulsion.* Dover Books on Physics. Dover Publications, 2006.

[19] Lorenzo Casalino. *Ottimizzazione Indiretta di Traiettorie Spaziali.*

[20] Lorenzo Casalino. *Equazioni in coordinate sferiche.*

[21] John E Prussing. «Primer vector theory and applications». In: *Spacecraft trajectory optimization* 29 (2010), p. 16.

[22] Wikimedia Commons. *File:Latitude and longitude graticule on a sphere.svg — Wikimedia Commons, the free media repository.* 2022. URL: https://commons.wikimedia.org/w/index.php?title=File:Latitude_and_longitude_graticule_on_a_sphere.svg&oldid=623468251.

[23] Solar System Dynamics NASA JPL. *Small-Body Element Tables.* 2021. URL: https://ssd.jpl.nasa.gov/sb/elem_tables.html#legend.

[24] Guido Colasurdo and Lorenzo Casalino. «Tentative Solutions for Indirect Optimization of Spacecraft Trajectories». In: *Space Engineering: Modeling and Optimization with Case Studies.* Ed. by Giorgio Fasano and János D. Pintér. Cham: Springer International Publishing, 2016, pp. 87–102.